2007

High Strength E-Glass/CNF Fibers Nanocomposite

Esam Abu-Zahra
Cleveland State University

HIGH STRENGTH E-GLASS/CNF FIBERS NANOCOMPOSITE

ESAM H. ABU-ZAHRA

Bachelor of Science in Mechanical Engineering

Amman College for Engineering Technology

June, 2001

Master of Science in Industrial and Manufacturing Engineering

Cleveland State University

May, 2003

Submitted in partial fulfillment of requirements for the degree

DOCTOR OF ENGINEERING at the

CLEVELAND STATE UNIVERSITY

December, 2007

This dissertation has been approved

For the **Department of Industrial and Manufacturing Engineering**

And the College of Graduate Studies by

_____

Dissertation Committee Chairperson, Dr. Taysir H. Nayfeh

Dept. of Industrial and Manufacturing Engineering/ _____

Department/Date

_____

Dr. Brian M. Thomas

Dept. of Industrial and Manufacturing Engineering/ _____

Department/Date

_____

Dr. Mounir B. Ibrahim

Dept. of Mechanical Engineering/ _____

Department/Date

_____

Dr. Majid Rashidi

Dept. of Mechanical Engineering/ _____

Department/Date

_____

Dr. Petru S. Fodor

Dept. of Physics/ _____

Department/Date

Dedicated to my parents, fiancé, brothers; Fuad, Nidal and Emad.

ACKNOWLEDGEMENT

I am delighted that I had a unique opportunity as a doctoral student to work on an industrial level project and to have been part of a dynamic team of experts with vast industrial and academic experience, supported by the university students.

I would like to express my sincere thanks and gratitude to my advisor and teacher, Dr. Taysir Nayfeh for giving me the opportunity to work on this phenomenal project at first and for his scientific guidance and encouragement throughout the course of this work at second. With his vast industrial and academic experience, along with his discipline and dedication, he geared the project to success exceeding our prospective and hopes.

Special thanks to Ms. Janet Hurst from the materials division of NASA Glenn Research Center for her guidance and analysis in both nanotechnology and fiber development. Janet, kindly, provided us with the scientific support we needed. My sincere thanks to Dr. Jim Leonard from GE lighting for his remarkable contribution to the project. He assembled and put to production the glass fiber-drawing machine at CSU. His insights to the theory development were very helpful.

I’am also grateful for all the hard work my co-workers put in. Tom Depietro, Dustin McCourt, Michael Wyban, Daniel Raible, Amanda Beach, Sagar Gadkari and Richard Bartel, I`am eternally grateful.

Last but not least, my heartfelt thanks goes to my family for their endless support and constant reminder of what a bright future I have.

CHAPTER I

INTRODUCTION

1.1 Background

The rising demand for lightweight and strong materials has prompted leading high-performance composites manufacturers to invest heavily in developing low cost and high strength new materials. Moreover, and given that the market has exploded worldwide, the need for additional capacity is sooner rather than later. Thus, there has been enormous activity in the field of nanocomposites to develop new materials with exceptional mechanical, electrical and thermal properties.

The outstanding mechanical properties of carbon nanotubes (CNTs) make them promising candidates in reinforcement applications. Although the ultimate goal is to utilize bare CNTs to produce continuous CNT fibers with the projected full strength of 150 GPa, the current limitations of the CNT material production technology is limiting the full utilization of the CNTs, in addition to the ultra high cost associated with the production of such fibers. As such, an intermediate alternative to the production of continuous strong nanotube fibers is to form hybrid matrices by combining the properties of the CNTs with those of another matrix to form a new nanocomposite material with much improved mechanical, thermal and electrical properties for the industrial use.

In general, the additional strength of the nanocomposite structure is the most sought out property by the end users. The added strength is however dependant on several factors, some of the factors that influence the nanocomposite strength include: volume fraction of the nano fiber material, the bonding interface strength between the fibers and the matrix, dispersion and alignment of the nano fibers in the composite matrix, and the micro defects in the structure especially the occurrence of voids and agglomerations.

Carbon and other types of nanotubes (10-20 nm diameters, 100 nm long) have extremely high strength, two to three orders of magnitude above that of normal engineering materials. However, because of their extremely high cost ($200-$500 /g), nanotubes are not typically used in industrial applications except in some extremely rare cases. On the other hand, carbon nanofibers (100nm diameters, 200 μm long) that are much weaker than nanotubes and cheaper ($100/lb) are finding wider use in industry. Their combined attributes of low cost, low density and high strength and stiffness is leading to the development of many new composite materials that are widely used in industry. Some of the CNFs composites applications include: super capacitors[3], energy storage devices and exterior and some interior parts of airplanes and ships.

1.2 The Research Problem

Nanocomposite materials have been attracting major attention for the last ten years because of their promise in developing extremely strong materials and the basic opportunities they present. Although there have been many advancements in the

manufacturing of nanocomposite materials, thus far, these processes have only been moderately successful in producing isotropic properties in polymer based nanocomposite matrices. In addition, few researchers have been exploring the development of metallic nanocomposite materials in part because of the misconception that the nanotubes will not survive the high temperatures that are required to process these materials.

In addition to the perceived restricted choices to the low processing temperature materials, there are still many shortcomings associated with the utility of nanotubes in nanocomposite materials. Some of the shortcomings include: poor dispersion of the nanomaterials primarily due to van der Waals forces, poor alignment and orientation of the nanofibers, also the difficulties associated with handling randomly oriented nanofibers in an industrial process.

Although in some cases researchers have been able to disperse the nanotubes in polymer based matrices and lately in a copper matrix, these efforts resulted in marginal improvements in the overall tensile strength and other properties relative to extremely high potential improvements that can be achieved. This in part is due to the fact that the phenomenal strength and electrical and thermal conductivities of the nanotubes are directed along their axial direction. Therefore, it is imperative that the nanotubes become aligned in the axial direction of the applied load and/or the conductivity direction in order to harness the maximum strength and conductivities in the structure of the nanocomposite material.

To this end, Nayfeh and Hurst[51] proposed a manufacturing methodology to use the fiber glass drawing process to align nanotubes/nanofibers in the glass fibers.

Later, their method was generalized to include other shapes and materials including aluminum, copper and titanium. In addition, in her previous research efforts, Hurst previously proposed and demonstrated that carbon and boron nitride nanofibers and nanotubes can survive high processing temperatures if encapsulated via hot pressing in vacuum in a glass matrix. She demonstrated that the nanotubes survived temperatures as high as 1600º C for at least one hour in an inert environment.

The Nayfeh-Hurst's method makes use of the high aspect ratio (length to width) of the CNFs along with the glass filament drawing process to imbed, disperse and align the CNFs in glass fibers. According to Nayfeh and Hurst, the shear forces acting on the dispersed CNFs in the glass matrix during the glass drawing process will align the nano fibers in the direction of flow. Moreover, the shear forces will disperse the existing inclusions in the glass fiber to minimize the effect of voids in the glass matrix.

Nayfeh and Janet projected that the combined effect of the micro fiber diameter along with imbedding, dispersing and orienting the CNFs in the glass will result in an extraordinary strong hybrid fiber. This method of reinforcing the glass fibers with CNFs offers an excellent intermediate solution for the industrial use of these materials.

The objective and scope of this research was to determine the feasibility of the Nayfeh-Hurst method and to quantify the potential gains in the mechanical strength of the nanocomposite glass fibers that were produced by using this technology.

To this end, three main experiments were conducted to study the effect of adding CNFs to E-glass during the glass forming process. The emphasis was on

studying the dispersion and the alignment of the CNFs in the glass matrix, as well as the glass fiber composite mechanical properties. The first two experiments involved using E-glass/CNFs coupons that were dropped in the glass melt during the forming process. In the last experiment, E-glass frit was successfully prepared and mixed with CNFs. Initially, the percent weight of the CNFs to be added to the frit mix was variable (2, 5 and 10)% by weight, but due to a catastrophic failure in the glass fiber drawing machine that resulted from some chemical reactions inside the melter, the experiment was conducted at only 5% wt. CNFs with the necessary mechanical and optical testing.

The overall results showed that the E-glass/CNFs nanocomposite fibers gained significant strength compared to pristine E-glass fibers; this is confirmed by tensile strength tests performed on the fibers. Electron microscopy confirmed that the CNFs were aligned in the glass matrix with non-uniform concentration along the length of the fibers. As was expected, because the feed stock (glass frit/CNFs) was in the powder from rather than hot pressed and encapsulated, the glass matrix was essentially doped with CNF's which was caused by the segregation of the CNFs from the glass frit due to differences in the specific gravities and the action of the nitrogen gas in blowing the light weight CNFs in the melter.

1.3 Document Organization

The material presented in this work is in the following order: chapter two gives a brief introduction to nanotechnology and carbon nanotubes (CNTs) in addition to glass fibers and glass fibers manufacturing process. Chapter three

provides a brief summary to the most recent related work in the nanocomposites area in general, and in ceramics and glass nanocomposites in particular. Chapter four gives a fundamental description of the analytical modeling and analysis.

Chapter five describes the experiment methodology and the feedstock preparation. Chapter six presents the results and the necessary analysis. Conclusion and recommended future work are presented in chapter seven.

CHAPTER II

BACKGROUND

2.1 Nanotechnology and Carbon Nanotubes

Nanotechnology is the creation of functional materials, devices, and systems through control of matter on the nanometer scale and the exploitation of novel phenomena and properties of matter (physical, chemical, biological, electrical, etc.) at that scale.[1]

Materials reduced to the nanoscale can suddenly show very different properties compared to what they exhibit on a macroscale, enabling unique applications.[2] For instance, opaque substances become transparent (copper); inert materials become catalysts (platinum); stable materials turn combustible (aluminum); solids turn into liquids at room temperature (gold); insulators become conductors (silicon)[2]. Materials such as gold, which is chemically inert at normal scales, can serve as a strong chemical catalyst at nanoscale[2]. Much of the fascination with nanotechnology stems from these unique quantum and surface phenomena that matter exhibits at the nanoscale. The discovery of CNTs has added a new dimension to the knowledge of nanotechnology in general and to carbon science in particular, which made them a key component of nanotechnology.[2]

2.1.1 Atomic Structure of Carbon Nanotubes

Carbon nanotubes (CNTs), which were discovered in 1991 by Iijima[3], are seamless hollow cylinders composed of well ordered sp^2-graphene sheets either in the form of single-walled (SW), multi-walled (MW) or Carbon nanofibers (CNFs) as shown in figure (2.1).

Carbon nanotubes can be visualized as a sheet of graphite that has been rolled into a tube. Unlike diamond, where a 3-D diamond cubic crystal structure is formed with each carbon atom having four nearest neighbors arranged in a tetrahedron, graphite is formed as a 2-D sheet of carbon atoms arranged in a hexagonal array. In this case, each carbon atom has three nearest neighbors.

The properties of nanotubes depend on the atomic arrangement or how the sheets of graphite are rolled, the diameter and length of the tubes, and the morphology, or nano structure[2]. (MWCNTs) are essentially concentric single walled tubes, where each individual tube can have different chirality. Secondary forces or Van der Waals bonding holds these concentric nanotubes together. CNFs have multiple concentric nested tubes with walls angled 20^0 to the longitudinal axis. While CNFs are similar to MWNTs, CNFs are not continuous tubes and their surfaces show steps at the termination of each tube wall[4] as shown in figure (2.1).

Both single and multi-walled nanotubes show unique properties that can be exploited for use in composite materials. Single-walled nanotubes are the most desired for fundamental investigations of the structure/property relationships in carbon nanotubes, since the intra-tube interactions further complicate the properties of carbon nanotubes, however, the high cost of SWNTs limits their applications on an industrial level (about $500/g, Nanotechnologies, Inc.).

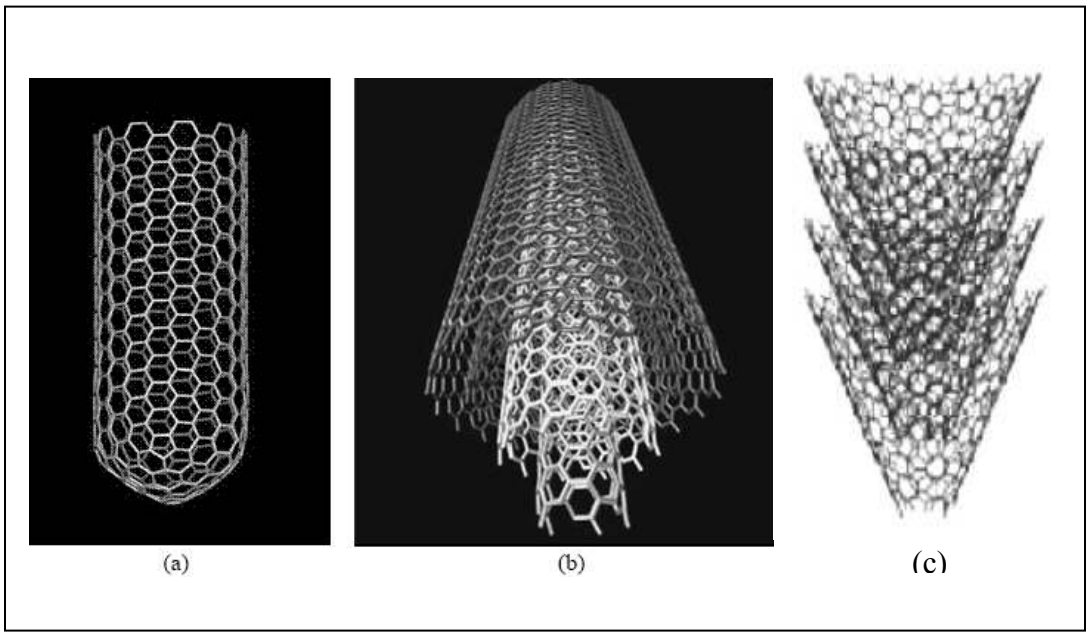

Figure (2.1) (a) Single Wall Nanotubes; (b) Multiwall Nanotubes; (c) Carbon Nanofibers. [4]

The atomic structure of nanotubes is described in terms of the tube chirality, or helicity, which is defined by the chiral vector and the chiral angle. Figure (2.2) shows a schematic of a carbon sheet where the adjacent carbon atoms are separated by the distance of about 0.14 nm , which is the length of the carbon-carbon/C-C bond, *lc-c*. A nanotube (NT) consists of many hexagonal carbon rings that have a width, *a*, of about 0.246 nm . These carbon rings are the structural cells in a NT. Different orientation of the carbon rings or cells determine their chirality and results in distinct NT structures (e.g., the “arm-chair” or “zig-zag” NTs).

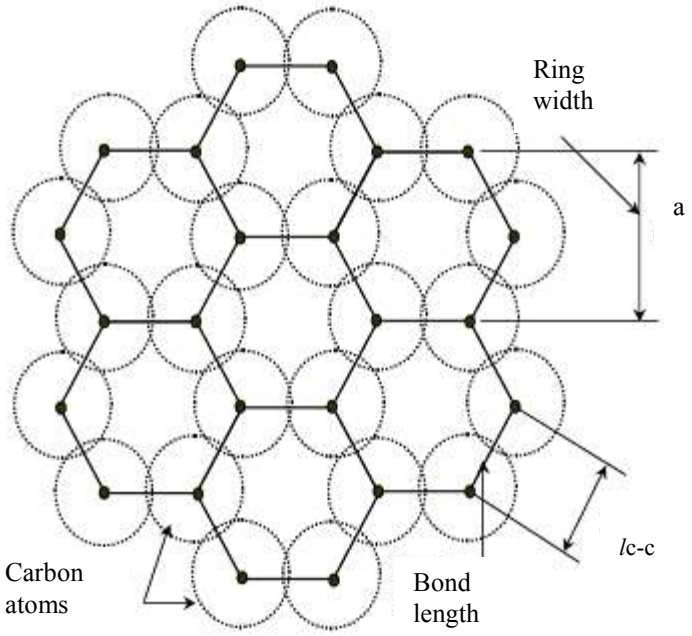

Figure (2.2) Schematic of a carbon lattice sheet composed of carbon atoms on a periodic hexagonal arrangement. [2]

The chirality of carbon nanotube has significant implications on the material properties. In particular, tube chirality is known to have a strong impact on the electronic properties. Graphite is considered to be a semi-metal, but it has been shown that nanotubes can be either metallic or semiconducting, depending on tube chirality.

The dimensions of CNTs/CNFs are nano scales with a high aspect ratio (length to diameter); table (2.1) gives a summary of the commercially available sizes[4].

	Length (μm)	Diameter (nm)
SWNT	0.2+	0.3-2

MWNT	1-50	10-50
CNF	30-100	100-200

Table (2.1) CNT/CNF physical sizes. [4]

2.1.2 Carbon Nanotubes Production Techniques

CNTs can be produced by arc discharge[3], laser ablation[6] or chemical vapor deposition (CVD) processes[7]. A summary of each method is presented hereafter.

2.1.2A Arc Discharge Method

In 1990, Krätschmer et al[3]. evaporated graphite rods by applying an ac voltage in an inert gas to produce fullerenes. Soon after, scientists applied a dc arc voltage between two separated graphite rods as shown in figure (2.3). The evaporated anode generates fullerenes in the form of soot in the chamber, and part of the evaporated anode is deposited on the cathode. In the cathode deposit, Iijima found the CNTs. In figure (2.3), after evacuating the chamber with a vacuum pump, an appropriate ambient gas is introduced at the desired pressure, and then a dc arc voltage is applied between the two graphite rods.

When pure graphite rods are used, the anode evaporates to form fullerenes, which are deposited in the form of soot in the chamber. These CNTs are made of coaxial graphene sheets and called multi-walled carbon nanotubes (MWNTs). When a graphite rod containing metal catalyst (Fe, Co, etc.) is used as the anode with a pure graphite cathode, single-walled carbon nanotubes (SWNTs) are generated in the form of soot.

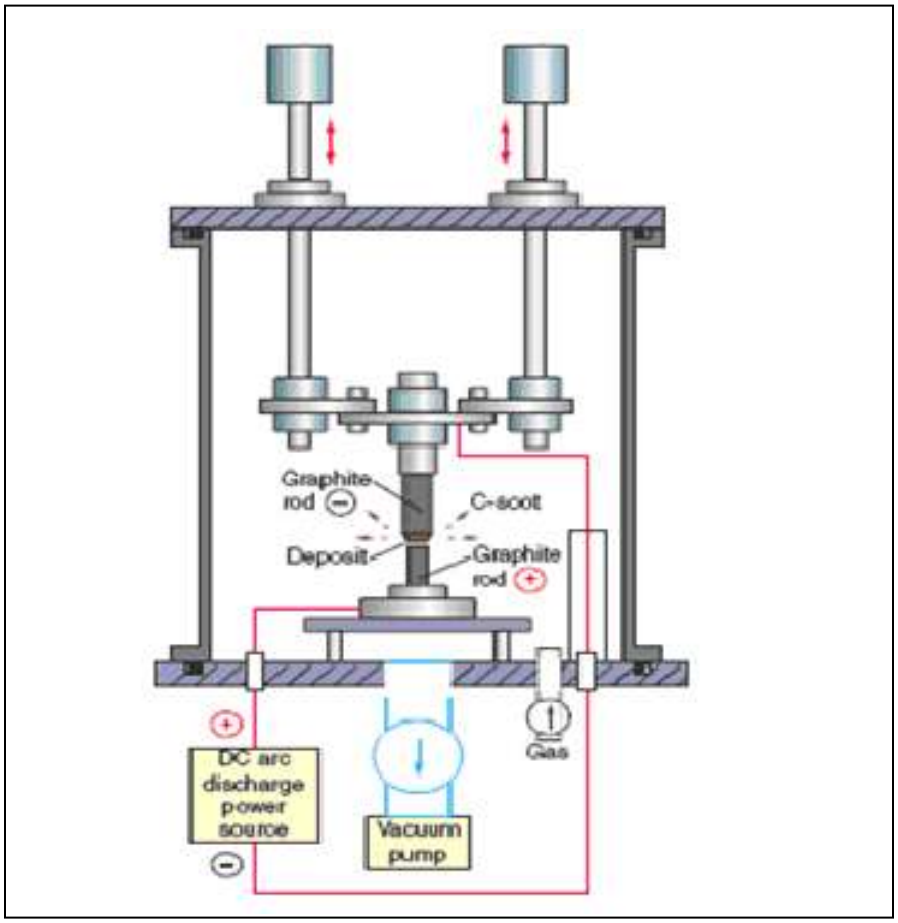

Figure (2.3) Schematic diagram of CNT formation apparatus by Arc Discharge Method. [3]

2.1.2B Laser Furnace

The Laser furnace method schematic diagram is shown in figure (2.4). The furnace consists of a quartz tube with a window, a target carbon composite doped with catalytic metals, a water-cooled trap, and flow systems for the buffer gas to maintain constant pressures and flow rates. A laser beam (typically CO2 laser) is introduced through the window and focused onto the target located in the center of

the furnace. The target is vaporized under inert conditions and results in the formation of SWNTs. The SWNTs produced are conveyed by the buffer gas to the trap, where they are collected. This method produces high quality SWNTs with the ability to control their diameter by changing the furnace temperature, catalyc metals, and flow rate of the inert gas.

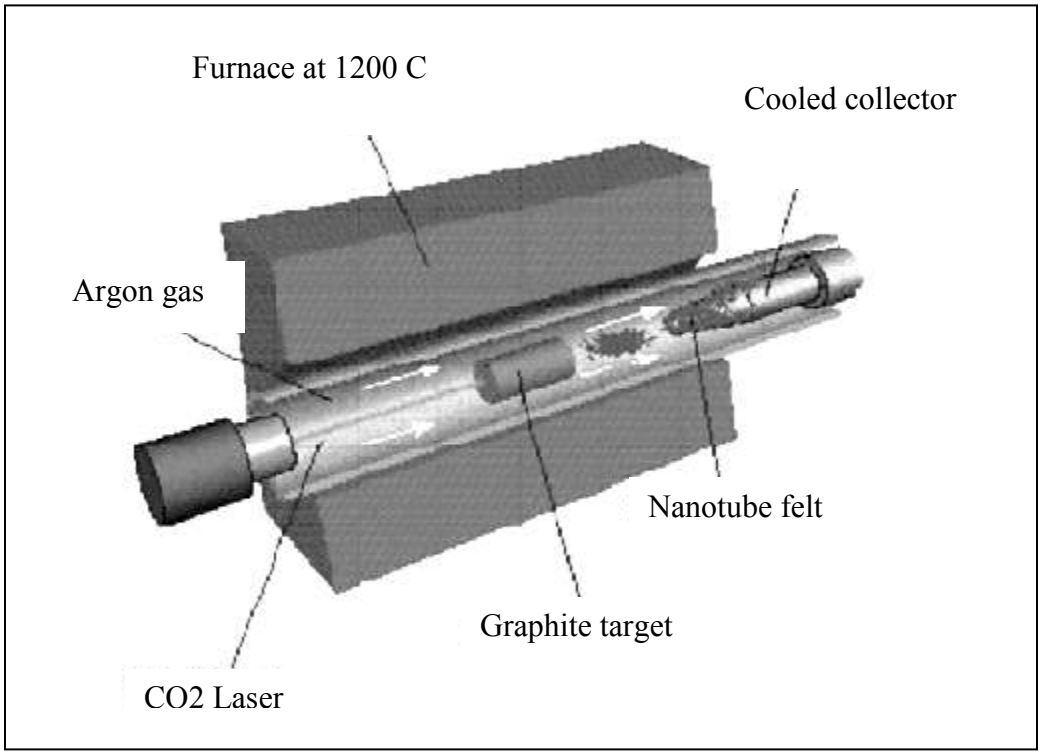

Figure (2.4) Laser furnace method.

2.1.2C Chemi

Chemical vapor deposition (CVD) is another popular method for producing CNTs in which a hydrocarbon vapor is thermally decomposed in the presence of a metal catalyst. The process of producing CNTs using this method involves passing a hydrocarbon vapor (typically for 15-60 minutes) through a tube furnace in which a catalyst material is present at sufficiently high temperature (600-1200°C) to

decompose the hydrocarbon. CNTs grow over the catalyst and are collected upon cooling the system to room temperature.

2.1.3 Carbon Fibers /Carbon Nanotubes Properties and Applications

Carbon Fibers are one of the most recent developments in the field of composite materials. It has been noticed that by binding synthetic fibers together with various resins, very light, strong and durable materials could be made[7]. Carbon fibers were originally developed for space technology, now they have been used in many other manufacturing areas, especially in material reinforcement applications. Due to their good mechanical properties, carbon fibers are in a very high demand, causing shortage of the fibers supplies as well as driving up the cost.

Carbon fibers are most notably used to reinforce composite materials, particularly the class of materials known as carbon fiber reinforced plastics (GFRP). This class of materials is used in aircraft parts, high-performance vehicles, sporting equipment, wind generator blades and gears and other demanding mechanical applications.

There are many different grades of carbon fibers available with different properties that can be used for different specific applications. Carbon fibers are composed of many featherweight strands, containing mainly carbon, usually embedded in an epoxy resin. For example, T-1000 carbon fibers are polyacrylonitrile (PAN) based resins. Table (2.2) shows some of the commercial carbon fibers and their properties[7].

Carbon Fiber	Tensile Strength (GPa)	Young's Modulus (GPa)	Density (g/cc)	Diameter (μm)
T-1000	6.9	290	1.79	5
T-800H	5.59	294	1.81	5.1
T-300	3.53	230	1.76	6.9

Table (2.2) Different carbon fibers properties. [7]

Large amount of research has been dedicated to the understanding of CNTs because of their extraordinary properties of high electrical and thermal conductivities, in addition to their outstanding mechanical properties as well as their unique structures. For example, SWCNTs exhibit metallic or semi-conduction depending on their graphene rolling up directions (helicity).

Thess et al.[6] measured an electrical resistivity of $< 10^{-4}$ ohm-cm at 300 K for metallic SWCNTs. Both metallic and nonmetallic properties are also observed for MWCNTs. As for the mechanical properties, several studies have described extraordinary high Young's modulus of above 1 TPa for both SWCNTs[8] and MWCNTs.[7]

Also, tensile strength of around 30 GPa[8] or more has been reported. On their thermal properties, experimental results and theoretical calculations reveal that the thermal conductivity is between 1800 and 6600 W/mK at room temperature[9], which matches and/or exceeds that of diamond (~ 2000 W/mK).

CNTs/CNFs are expected to be used in four main fields due to their superior properties, as shown in figure (2.5), which are:

1. CNTs are suitable as electron field emitters for microscopic probes or field emission displays because of their nanometer-sized needle like shape, high electrical conductivity and high chemical and thermal stability.
2. Electronic devices for nanometer-sized transistors, diodes and logic circuits are considered. These are expected to replace silicon device technologies in the future.
3. The use of electrochemical functions such as super capacitors for energy storage, hydrogen storage for fuel cells and various sensors is proposed.
4. CNT incorporated composite materials are widely investigated to improve or induce structural, electrical and/or thermal functions. The last application field is introduced in the next section.

There are mainly three fields for CNTs for the use in nanocomposite materials. The first is the mechanical reinforcement of a matrix by CNTs because of their high strength. The second is the improvement of thermal conductivity by introducing high thermal conductive CNTs. The third is the introduction of electrical induction by the percolation of CNTs in the matrix. In these applications, the low weight nature of CNTs as well as their high aspect ratio provides further advantages for their use as filler materials. So far CNTs have been intensively used by not only polymer-based composites but also metal and ceramic matrix systems.

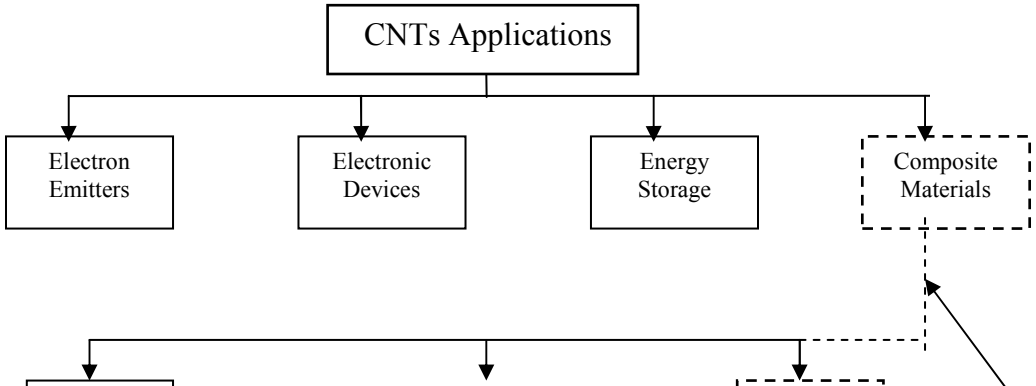

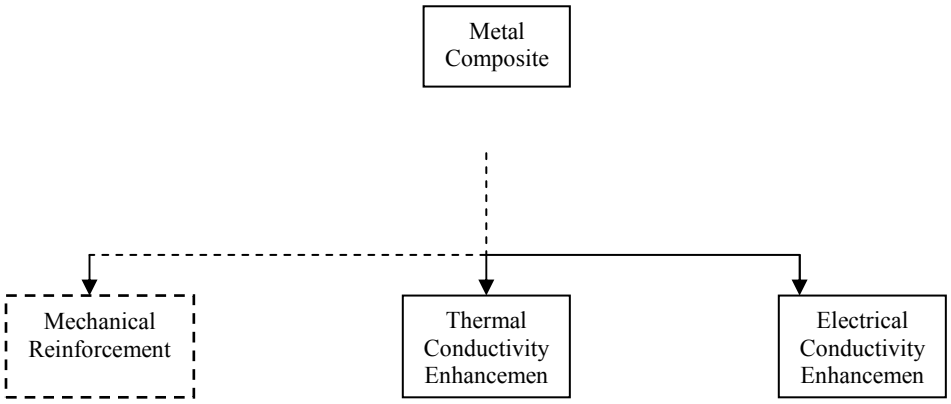

Figure (2.5) CNTs Applications

2.1.4 CNTs Composites Toughening Mechanism

Ye, Lam et. al[10] described two toughening mechanisms that occur during the SWNT strengthening process. First, the fibers experience the crazing. The initiation of the crazing can be a notch defect or an impurity at the fiber surface where stress concentration forms easily, as shown in figure (2.6a). A crazing starting from surface and ending in fiber is noted by an arrow in figure (2.6b). Instead of crack extension, the crazing extension is preferred for materials with a low entanglement density.

The presence of CNTs [figure (2.6b)] does not block the crazing, due to the small size of MWNTs and SWNTs applied (10 nm and 1.3 nm in average diameter, respectively). However, the CNTs hinder the crazing extension because both

alignment of CNTs in the crazing area and slippage between CNTs consume extra energy [figure (2.6c)]. The retarded crazing extension can therefore contribute to a higher tensile strength.

Incase SWNTs are homogeneously distributed in composite fibers, the possibility of stress concentration is greatly reduced. Tensile stress is transferred uniformly along the fibers, causing the formation of regularly arranged crazing, as demonstrated in figure (2.6c). Each crazing area has a lower number of fibrils and larger tensile resistance. Such a fiber with few weak points can be very strong. At the second stage [figure (2.6d)], the crazing fibrils break and CNTs reinforce the composite fibers by the pull-out mechanism. This is an important reinforcement process because by partly replacing the crazing fibrils, CNTs strengthen the weakest part of the fiber.

Due to the superior tensile strength of CNTs, the tensile stress may be fully transferred to CNT-matrix interfaces, instead of breaking the CNTs. Therefore, the reinforcement effect depends on the interfacial adhesion between CNTs and the matrix.

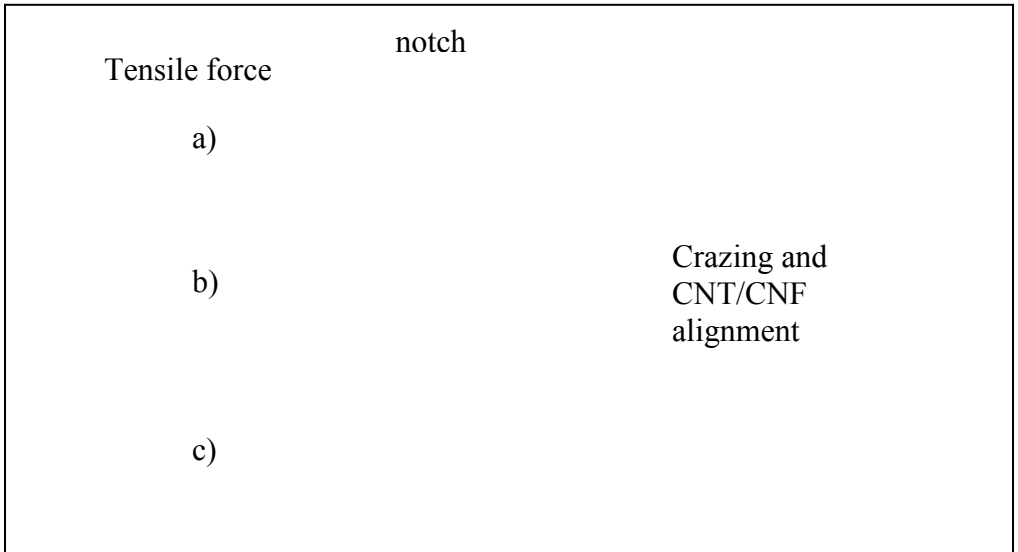

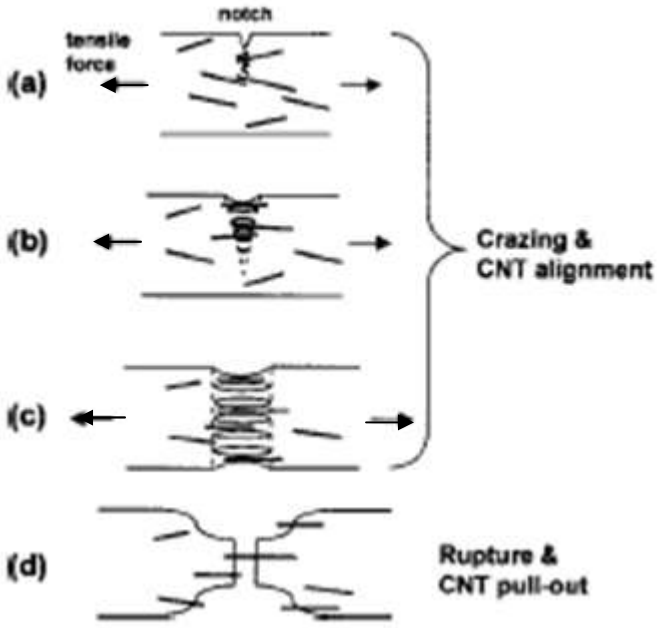

Figure (2.6) Schematic illustration of the crazing and rupture of a CNT-PAN composite fiber under tension. [10]

In the case of polymer based CNTs nanocomposites, there exist two advantages for material processing. One is the dispersion of CNTs into the polymers, that is, liquid polymers can facilitate the deagglomeration and dispersion of CNTs greatly by sonication. The other advantage is the lower heat treatment temperature for the solidification of polymers, which prevents the CNTs from being structurally damaged during processing. In addition to these processing advantages, the big differences in their material properties between CNTs and polymers such as mechanical strength, thermal conductivity and electrical conductivity can provide large gain in their characteristics in polymer/CNT nanocomposites.

Composite materials consisting of a metal matrix with CNT fillers have also been investigated for the improvement of the mechanical properties of metals,

however, the high porosity of the nanocomposite remains a problem. For example, Kuzumaki et al[11] prepared Al/MWCNT (5 vol %) composites by hot-pressing and hot-extrusion methods at 500 – 600 °C from the powder mixtures.

The incorporation of CNTs into ceramics is also expected to induce or improve several functions, however, their conventional powder technological techniques including powder mixing and high temperature sintering may cause the CNTs to lose their integrity which is necessary to fulfill their function in the matrix. That is, the material design of ceramic-matrix CNT composites is more challenging than that of polymer and metal systems.

CNT/ceramic composites developed up to now have shown much lower mechanical properties than expected, and in some cases, even worse mechanical properties than those of the monolithic ceramic matrices. This is mainly due to the inhomogeneous distribution of CNTs within the ceramic matrix and the weak interfacial bonding between CNTs and the matrix.

2.2 Glass Fibers

There is a distinct difference between Glass Fibers and Fiberglass. Fiberglass is only one of the products that can be made from glass fibers. Glass fibers can be used in not only fiberglass, but also draperies, clothing, and other industrial applications.

Four billion pounds of glass fibers are used annually. The market for glass is growing, while the inventories are low, and the prices are high. This means that some companies are using less glass in their products, thus resulting in a lower quality product[37].

Glass fibers fall into two categories, low-cost general-purpose fibers in which over 90% of all glass fibers are general purpose products[41], these fibers are known as E-glass fibers, and premium special-purpose fibers, these include: S-Glass which is used whenever high strength is required, C-Glass used for high chemical durability, ECR-Glass used for high corrosion resistance purposes, and D-Glass is used for low dielectric applications.

Two generic types of E-glass are known in the market today[42]. The present E-glass which contains 5 to 6 % wt. of boron oxide, and the boron oxide free E-glass. Severe environmental regulations require the addition of costly emission abatement systems to eliminate the boron. Alternatively, the use of environmentally friendly boron-free E-glass is favorable in which the melts do not contain, and therefore do not emit, boron into the environment during processing.

Glass fibers are used in many applications, such as:

- Aerospace and Space suits

Due to its lightweight, strength, impact resistance and non-flammable properties, fiber glass is used to reinforce aircraft laminates, luggage bins and other composite structures.

- Automotive Industry
- Construction: For a broad range of construction materials such as roofing shingles, bathtubs, shower stalls and window frames, fiber glass's strength and durability make it the preferred reinforcement material.
- Corrosion

Fiber glass helps curb corrosion in a variety of applications. Rust-proof bridge decking.

- Electronics: Glass fiber reinforced circuit boards
- Filtration: Air purification
- Sports & Recreation

2.2.1 Glass Fibers Manufacturing Process

The French scientist, Reaumur, considered the potential of forming fine glass fibers for oven glass articles as early as the 18th century. Continuous glass fibers were first manufactured in substantial quantities by Owens Corning Textile Products in the 1930's for high temperature electrical applications[15]. The manufacturing process for continuous glass fiber production is called fiber glass drawing and it is illustrated in figure (2.7).

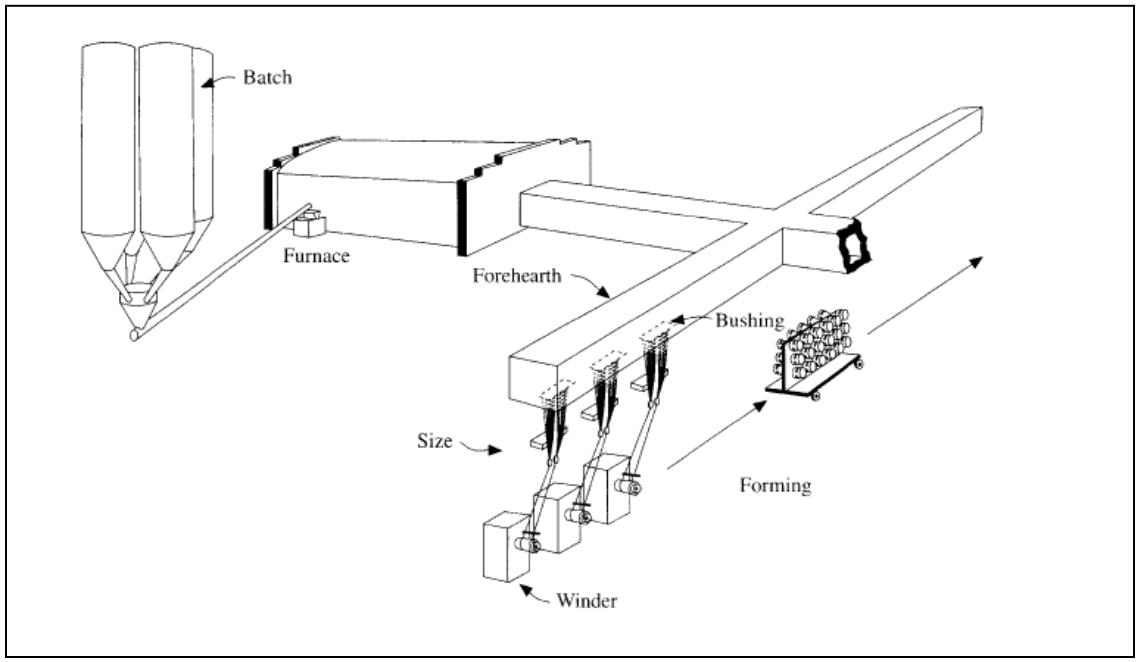

Figure (2.7) Continuous glass fiber manufacturing process. [16]

Raw materials such as silicates, soda, clay, limestone, boric acid, fluorspar or various metallic oxides are blended to form a glass batch which is melted in a furnace and refined during lateral flow to the fore hearth[16]. The molten glass flows to platinum/rhodium alloy bushings and then through individual bushing tips and orifices ranging from 0.76 to 2.03 mm (0.030 to 0.080 in) and is rapidly quenched and attenuated in air (to prevent crystallization) into fine fibers ranging from 3 to 35 μm. Mechanical winders pull the fibers at linear velocities up to 61m/s over an applicator which coats the fibers with an appropriate chemical sizing to aid further processing and performance of the end products. High strength glass fibers like S-2 Glass are compositions of aluminosilicates attenuated at higher temperatures into fine fibers ranging from 5 to 24 μm. Several other types of silicate glass fibers are manufactured for the textile and composites industry.

The final glass fiber diameter is determined by many factors, most importantly, the drawing speed, other factors include: the bushing temperature, glass viscosity, and the pressure head over the bushing[41].

2.2.2 Glass Fibers Drawing Model

The fiber forming process can be represented in a cylindrical coordinate system (r, θ, z) as shown in figure (2.8), where z is the axial distance measured from the tip exit and is positive in the pulling direction, the direction of gravity. The radial direction r is measured from the axis of the jet. The fiber forming process is axisymmetric and independent of the polar angle θ.

The following equations describe the following flow fields: axial velocity $V(z)$(m/s), temperature $T(z)$ (°C), filament radius $r(z)$ (mm), and axial stress $\sigma(z)$(MPa) for a given set of processing conditions: tip radius-R_o, tip temperature-T_{tip}, mass flow rate-W (kg/hr), and fiber velocity- V_l (m/s), and a given set of glass properties: density-ρ (kg/m^3), viscosity-$\eta(T)$ (Pa.s), heat capacity-c_p (J/kg/°C), emmisivity- ε, etc.). A one-dimensional model, which assumes that the velocity, temperature and pressure fields inside the glass jet to have no radial dependence, was used in the analysis. This assumption is justified only in the central region of the jet where the slope of the jet surface is less than 0.1. The governing equations were mainly derived form Glicksman[48] and Gupta[49].

The initial velocity of the molten glass through the tip follows Hagen-Poiseuille law, given by

$$V_o = \frac{(\rho g H + \sigma_{tip}) R_o^2}{8 L_o \eta_{T_o} \left(1 + \frac{3\pi R_o}{8 L_o}\right)} \tag{2.1}$$

Where the viscosity η_{T_o} is calculated at the tip bore temperature T_o.

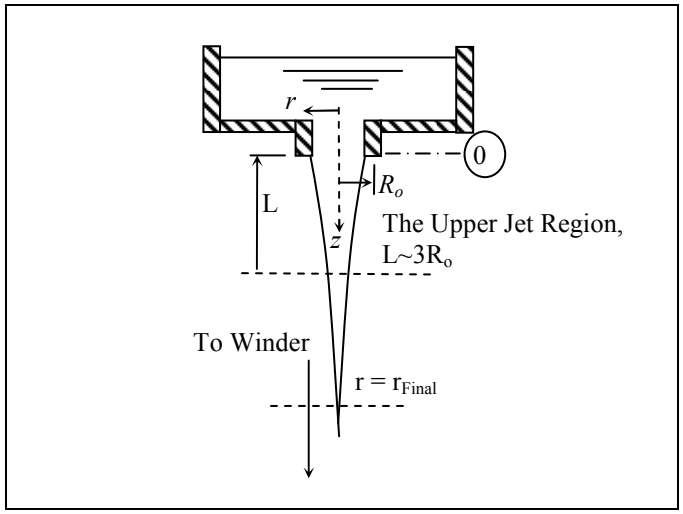

Figure (2.8) The jet diagram

The viscosity η (Pa.s) follows Vogel-Fulcher-Tamman (VFT) equation given by:

$$\eta(T) = \exp\left[2.303\left(\eta_A + \frac{\eta_B}{(T - \eta_{T_o})} - 1\right)\right] \tag{2.2}$$

Where η_A,η_B, η_{To} are viscosity constants

2.2.3 Glass Fibers Chemical Composition and Physical Properties

Chemical composition variation within a glass type is caused by differences in the available glass batch raw materials, or in the melting and forming processes, or from different environmental conditions at the manufacturing site. These compositional fluctuations do not significantly alter the physical or chemical

properties of the glass type. However, tight controls are typically maintained within a given production facility to achieve consistency in the glass composition for production capability and efficiency[15]. Table (2.3) provides the oxide components and their weight ranges for eight types of commercial glass fibers.

	Glass Type							
	A	C	D	E	ECR	AR	R	S-2
Oxide	%	%	%	%	%	%	%	%
SiO2	63-72	64-68	72-75	52-56	54-62	55-75	55-60	64-66
Al2O3	0.6	3-5	0.1	12-16	9-15	0-5	23-28	24-25
B2O2	0.6	4-6	21-24	5-10		0-8	0-0.35	
CaO	6-10	11-15	0.1	16-25	17-25	1-10	8-15	0-0.2
MgO	0.4	2-4		0.5	0.4		4-7	9.5-10
ZnO					2-5			
BaO		0.1						
Li2O						0.15		
Na2O+K2O	14-16	7-10	0.4	0.2	0.2	11-21	0.1	0-0.2
TiO2	0-0.6			0-0-1.5	0.4	0.12		
ZrO2						1.18		
Fe2O3	0-0.5	0-0.8	0-0.3	0-0.8	0-0.8	0.5	0-0.5	0-0.1
F2	0-0.4			0.1		0.5	0-0.3	

Table (2.3) Composition ranges for glass fibers. [15]

Glass fiber properties, such as tensile strength, Young's modulus, and chemical durability, are measured on the fibers directly[17]. Other properties, such as dielectric constant, dissipation factor, dielectric strength, volume/surface resistivities, and thermal expansion, are measured on glass that has been formed into a bulk sample and annealed (heat treated) to relieve the forming stresses. Properties such as density and refractive index are measured on both fibers and bulk samples, in annealed or unannealed form.

Table (2.4) gives the most known mechanical properties for different types of glass fibers.

	Glass Type								
	A	**C**	**D**	**E**	**ECR**	**AR**	**R**	**S-2**	**Silica**
Density, gm/cc	2.44	2.52	211	2.58	2.72	2.7	2.54	2.46	2.15
Refractive Index	1.538	1.533	1.463	1.558	1.579	1.562	1.546	1.52	1.458
Softening Point ^{o}C	705	750	771	846	882	773	952	1056	
Annealing Point ^{o}C		588	521	657				816	
Strain Point ^{o}C		522	477	615			736	766	
Tensile Strength (MPa)									
23 ^{o}C	3310	3310	2415	3445	3445	3241	4135	4890	3400
371 ^{o}C				2620	2165		2930	4445	
Young`s Modulus (GPa)									
23 ^{o}C	68.9	68.9	51.7	72.3	80.3	73.1	85.5	86.9	69
53 ^{o}C				81.3	81.3			88.9	
Elongation (%)	4.8	4.8	4.6	4.8	4.8	4.4	4.8	5.7	5
Melting Temp ^{o}C				1200	1159			1500	1670

Table (2.4) Mechanical properties of glass fibers. [15]

CHAPTER III

LITERATURE REVIEW

3.1 Introduction

Since the discovery of CNTs/CNFs and the realization of their unique physical properties, including mechanical, thermal, and electrical, many researchers have endeavored to fabricate advanced CNTs/CNFs composite materials that exhibit one or more of these properties.

Although most of the research has focused on the development of nanotube based polymer composites, attempts have also been made to develop metal, and glass matrix composites with nanotubes as reinforcement. In this chapter, an overview in the recent developments of the nanocomposites, with the emphasis on glass nanocomposites, will be presented, along with all the challenges accompanied to this research.

3.2 Polymer Nanocomposites

Currently, carbon nanotubes are being dispersed in polymer matrices using melt processing, solution processing, or in-situ polymerizations. Property enhancements include strength, stiffness, thermal stability, solvent resistance, glass transition temperature, electrical conductivity, reduced thermal shrinkage as well as optical anisotropy. The presence of SWNTs can also influence polymer crystallization. In addition, carbon nanotubes are over 10^5 times more resistant to electron radiation than polyethylene and about 10^3 times more resistant than radiation resistant rigid-rod polymers such as poly (p -phenylene benzobisoxazole)[18].

Thaliyil et. al[19] Noticed that by adding 10wt.% SWNT to PAN (Polyacrylonitrile) fibers, the composite matrix exhibit a 100% increase in the tensile modulus at room temperature. The hybrid carbonized and activated PAN/SWNT films are very promising for supercapacitior electrode applications. Table (3.1) summarizes their results:

SWNT (WT. %)	Tensile Modulus (GPa)	Tensile Strength (GPA)
0	7.9	0.23
5	14.2	0.36
10	16.2	0.36

Table (3.1) PAN/SWNT composite properties. [19]

Saish Kumar[18] studied adding SWNT to PBO (Poly-phenylene benzobisoxazole). (PBO) was synthesized in the presence of single wall carbon nanotubes (SWNTs) in polyphosphoric acid (PPA) using typical PBO polymerization

conditions. PBO and PBO/SWNT lyotropic liquid crystalline solutions in PPA were then spun into fibers using dry-jet wet spinning. The tensile strength of the PBO/SWNT fiber containing 10 wt.% SWNT was shown to be over 50% higher than that of the control PBO fibers containing no SWNT. Table (3.2) summarizes the test results:

Sample	Tensile Modulus (GPa)	Tensile Strength (GPa)
PBO	138	2.6
PBO/SWNT (95/5)	156	3.2
PBO/SWNT (90/10)	167	4.2

Table (3.2) PBO/SWNT composite properties. [18]

Sandler et al.[40] prepared epoxy/MWCNT composites by shear-intensive mechanical stirring of the mixture and following solidification via a hardener at 140 °C for 8 hours. They measured the electrical conductivity of the epoxy/MWCNT composites by AC impedance spectroscopy and observed the electrical percolation threshold to be below 0.005 wt.% of CNT content with an electrical conductivity increase of 106 S/cm. Their comparative materials of epoxy/carbon black composites reveal the percolation threshold to be 1.0 wt.%, which defines the effect of CNTs clear for electrical fictionalization.

Biercuk et al[20] and Choi et al.[21] respectively described an increase in the thermal conductivity by 125 % with 1 wt.% SWCNTs and by 300 % with 3 wt.%

SWCNTs concentration in the epoxy/SWCNTs nanocomposites compared to the pure epoxy material.

Gojny et al.[22] investigated the fracture toughness behavior of similar composites and obtained an increase of 25 % with the incorporation of 1 vol. % double-walled CNTs. Qian et al.[23] They also reported an improved mechanical strength and modulus of polyethylene with 1 wt.% MWCNT incorporation. On the other side, Lau et al.[41] observed enlarging holes at the interfaces between MWCNTs and the epoxy matrix during fracturing as shown in figure (3.1). In their composite materials, no benefit of CNTs on the mechanical performance was obtained because embedded CNTs were easily pulled out from the matrix. Consequently, they pointed out that the interfacial bonding between CNTs and the matrix is quite important and to be a critical issue for the mechanical reinforcement of the materials.

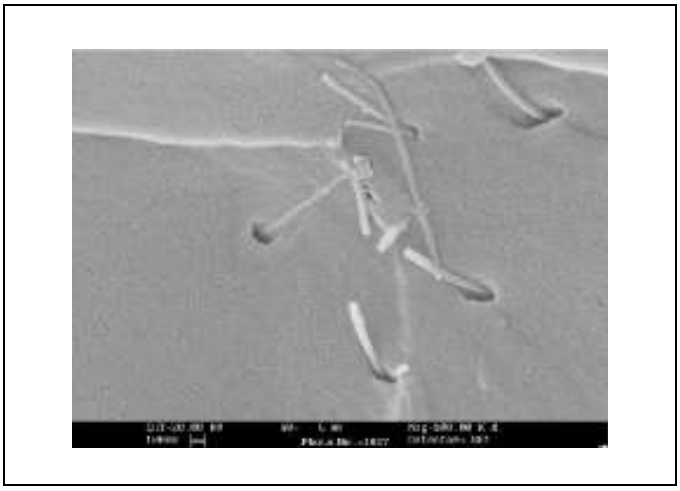

Figure (3.1) SEM image of the fracture surface of epoxy/CNT composite containing 2 wt% MWCNTs. The holes at the interface reveal weak bonding of MWCNTs to the epoxy matrix. [22]

3.3 Glass Nanocomposites

As mentioned earlier, the material design of glass matrix CNT composites is more challenging and requires more preparations of the materials involved. This is mainly because in the case of CNT/Glass composites, the toughening mechanism is highly dependent on the interface area between the material and the CNTs. To this end, some scientists studied the effect of treating the CNTs before dispersing them in the matrix.

Boccaccini, Acevedo et, al.[24] studied the effects of adding MWCNT into a Duran borosilicate glass matrix as a reinforcing element. Duran glass consist of 81% of SiO_2 ,13% of B_2O_3 and some other elements, such as: Al_2O_3 and Na_2O.

The authors reported that the presence of Alumina in the chemical composition of Duran glass is highly favorable since it should prevent the glass from crystallization. (E- glass that is used in this research has (12-16) % Alumina).

Chemical Composition (wt. %)	
SiO2	81
B2O3	13
NA2O+K2O	4
Al2O3	2
Physical Properties	
Density (g/cm^3)	2.23
Modulus of Rupture (MPa)	60
Elestic Modulus (GPa)	64
Refractive Index	1.473

Table (3.3) Duran glass characteristics

The CNTs employed as the reinforcing phase were multi wall with diameters between 10- 40 nm with a 10 wt.% in the mixture. The experiment was

carried out in two cases: in the first case, CNTs were dispersed in a water solution containing 10 wt.% of a surfactant and the dispersion was ultrasonicated for 2 hours. Duran glass powder was added and the final mixture, called mixture A, was sonicated for 2 hours. In the second case, CNTs were dispersed in a water/ethanol solution containing 10 wt.% of Triton, etraethoxysilane and NaOH. The dispersion was ultrasonicated for 2 hours. Duran glass powder was then added and the final mixture, called mixture B, was ultrasonicated for 2 hours.

In both cases, initial results showed that the glass powder and the CNTs agglomerate together with some glass powder that's not in contact with CNTs. The agglomerates in mixture B in figure (3.2b) seem to be smaller than those in mixture A in figure (3.2a), but they are more numerous.

In the agglomerates of the mixture B, the authors suggest that it is probably due to the introduction of a SiO2 interface between the CNTs and the glass, a rather homogeneous mixing was found, as shown in Figure (3.3). The surface modification of CNTs is thus found to be useful, even though not sufficient to ensure a complete homogenization of the CNT/glass powder mixture. This result agrees with literature reports considering the need to modify the surface of CNTs in order to improve their dispersion in glass matrices.

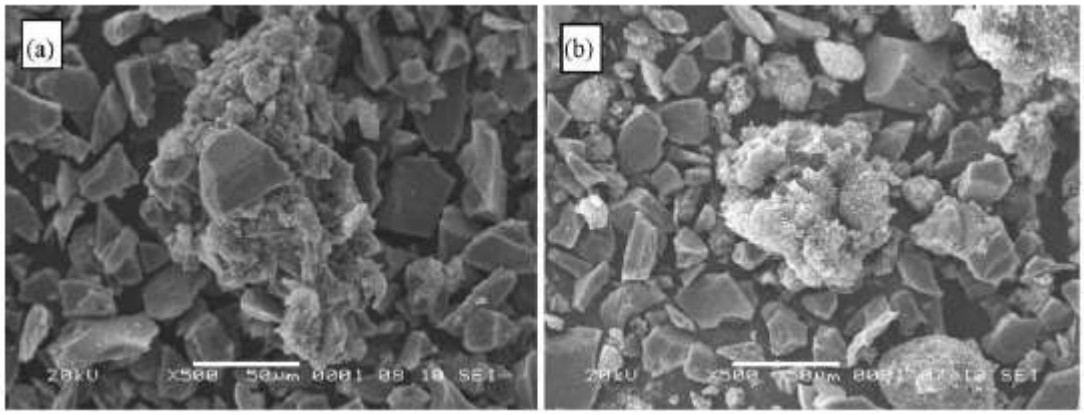

Figure (3.2) Agglomeration in matrices A and B. [24]

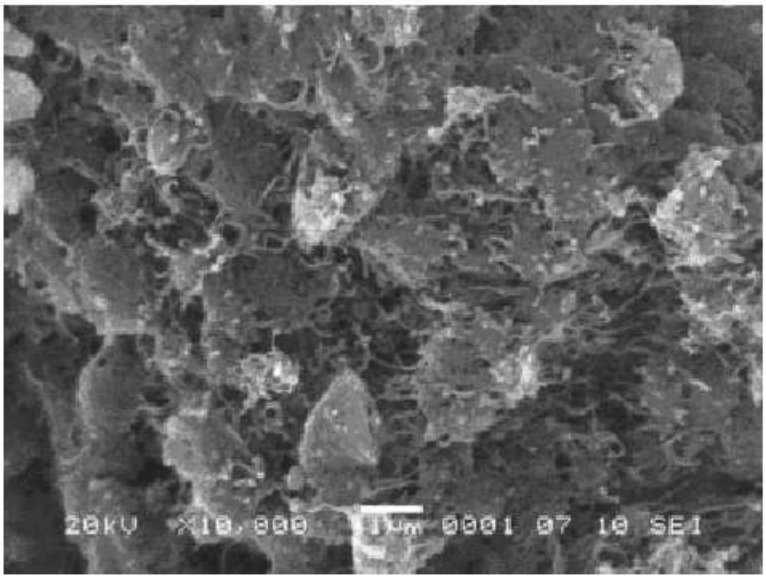

Figure (3.3) SEM Micrograph at high magnification of CNTs/glass in the mixture. [24]

In the previous study, it has been shown that the presence of CNTs decreases the sintering ability of the glass matrix, which is thought to be due to the huge aspect ratio of the rigid, non-sintering inclusions causing a dramatic increase of the effective viscosity of the system at the sintering temperature. The relatively poor homogenisation of the CNTs/glass mixtures used, probably hinders significant

improvement in the mechanical properties of the composites, especially fracture toughness, despite the possibility of CNT pullout from the glass matrix. The coating of the surface of CNTs with silica, developed by the sol–gel method, was found to be promising to increase the homogeneity of CNT/glass powder mixtures and the density of composites made from them.

Ninj, Zhang et. al.[25] studied the improvement in mechanical properties by adding MWCNTs (20 to 40 nm in diameter and tens of microns in length) to SiO2 glass powder. CNT/SiO2 composites were mixed by ultrasonication in an ethanol solution and fabricated by direct mixing and hot pressure sintering at 1300 C.

The diameter scope of SiO2 particles is shown in the following table:

	Scope of Diameter (μm)							
	<0.5	**<1**	**<2**	**<5**	**<7**	**<10**	**<15**	**<25**
Accounted weight ratio (wt. %)	8.2	21.4	41	65.3	77.4	87	92.9	100
Median diameter	3.1							

Table (3.4) The diameter scope of SiO2 particles used. [25]

The results of this work are shown figure (3.4) where the dependence curves of bending strength and the fracture toughness are plotted against CNT volume content. The bending strength and the fracture toughness increase with the CNTs volume increase, up to a volume content of 5 vol.% CNT, however, when the volume content of CNT is greater than 5%, the bending strength and fracture toughness decrease with the increase of CNT.

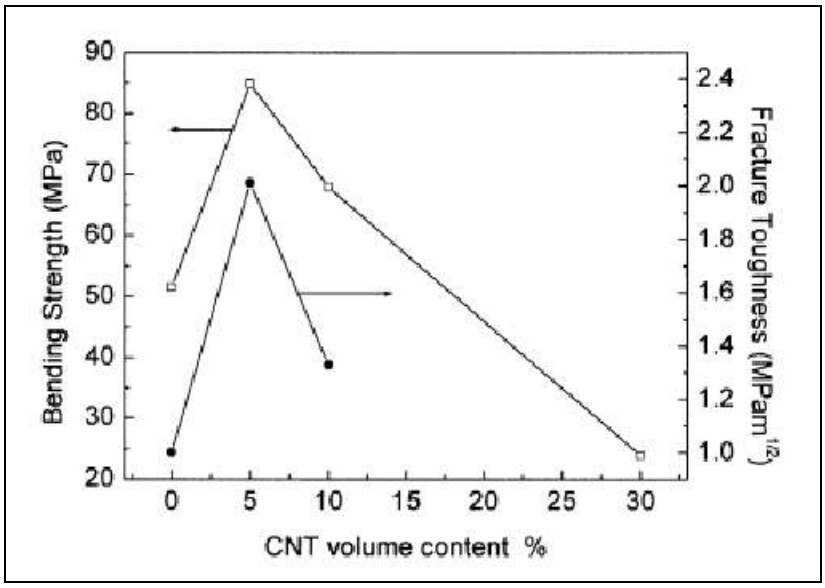

Figure (3.4) Bending strength/fracture toughness vs. CNT vol.%. [25]

According to the authors, two contrary factors may result in the above phenomena. First, CNTs have large aspect ratio and excellent mechanical properties. According to the theory of short fiber reinforced composites, it can improve the mechanical properties greatly. On the other hand, CNTs make the bending strength decrease because they can hinder the densification. With the increase of CNT content, the probability to agglomerate is increased.

When the stress transfer to the CNTs, it's easy to separate them from the matrix, which reduces the mechanical properties. As shown in figure (3.5a and b) there are more pullouts and longer CNTs on the fracture surface can be found in the sample with 10 vol.% CNT than that of the sample with 5 vol.% CNT.

TEM images show that breakage and clear pulling out of CNTs occurred on the fracture surface of the samples. The authors justified that by assuming that there were some defects on the surface of the CNTs before running the experiment or during the experiment after the heat treatment. These defects may reduce the

stiffness of the CNTs. Moreover, it's suspected that the clear puling-outs may come from the agglomeration of CNTs.

.

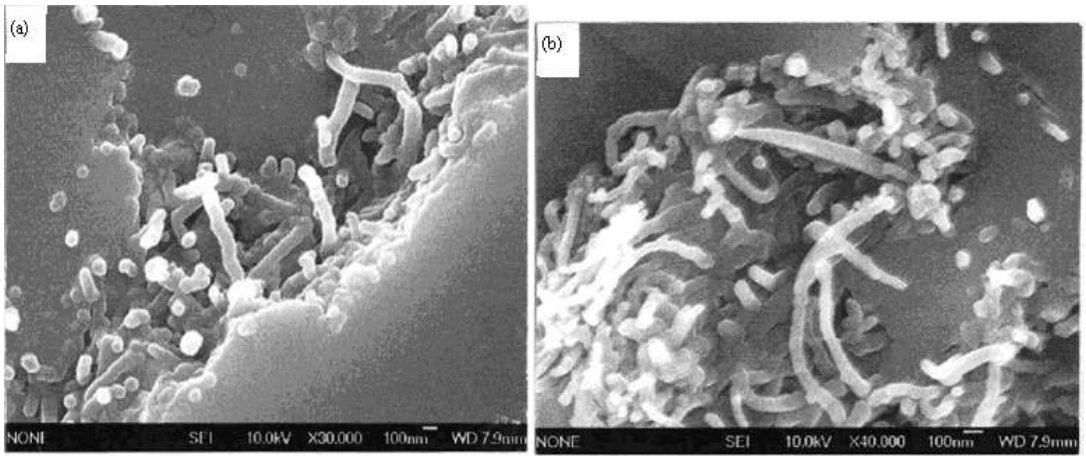

Figure (3.5) Fracture surface of (a) 5 vol.% CNT/SiO_2 composite (b) 10 vol.% CNT/SiO_2 composite. [25]

By looking at the SEM micrographs of the fracture surface in figure (3.6), it's noticed that the dispersion of CNTs in the matrix is not homogenous which may also reduce the strengthening role CNTs. More research is needed to improve the homogeneity of CNTs in the matrix.

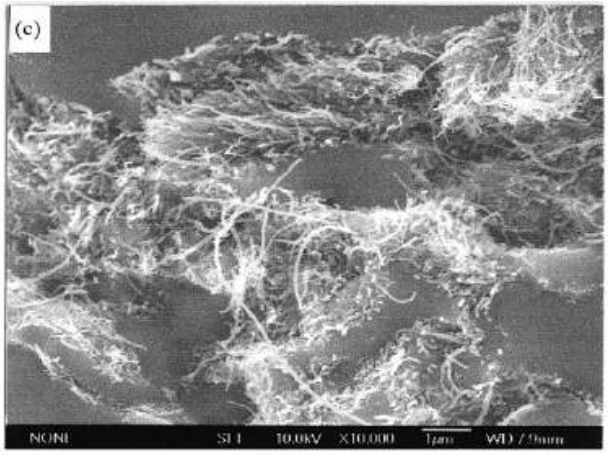

Figure (3.6) Nonhomegenouse distribution of the CNTs in the SiO_2 matrix. [25]

Katsuda, Gertsel et. al.[26] studied the effect of adding MWCNTs to a Si-C-N glass matrix. Two types of MWCNTs type A and type B were used for the glass reinforcements. Type A CNTs are smaller in diameter and relatively longer than the type B ones (higher aspect ratio). Type B CNTs have stuffed structure inside with distinctive grapheme sheets indicating an amorphous nature in the majoity. The contents of CNTs in the Si–C–N nanocomposites were adjusted from 0 to 2 in mass %, which corresponds approximately to the volume content (vol. %)

Fracture toughness (KIc) for the Si-C-N nanocomposites was tested for both CNTs types. Figure(3.7) shows the results. It can be noted that the incorporation of type A-CNT significantly increases the fracture toughness of Si–C–N glass even at a content as low as 1 mass %. With a content of 2 mass %, the increase of KIc reaches more than 60% as compared to the pure Si–C–N material. On the other hand, the addition of type B-CNTs has no effect on the fracture toughness as revealed by behavior similar to that of the pure material.

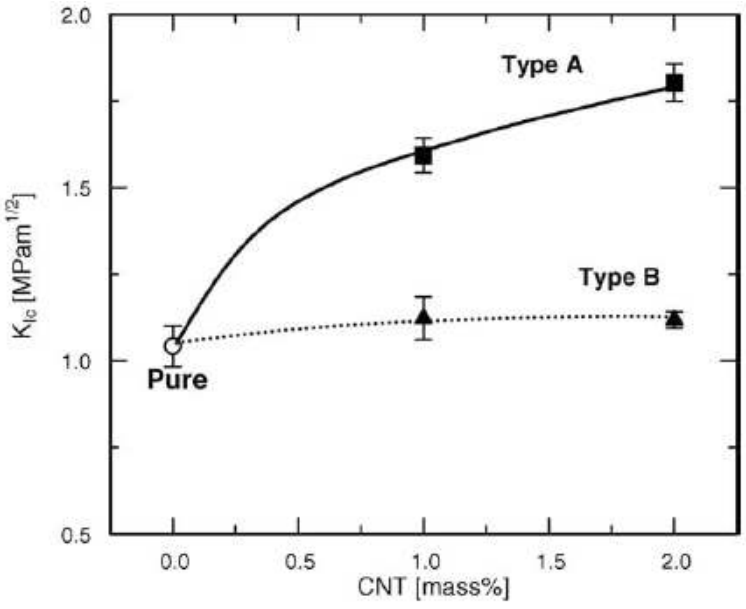

Figure (3.7) Fracture toughness behavior of Si-C-N nanocomposite as a function of the CNT content. [26]

It is confirmed by the authors that there are no significant differences in the bulk density, Young's modulus, Poisson's ratio and coefficient of thermal expansion (CTE) among the materials prepared in this study. That is, the addition of CNTs up to 2 mass% does not influence the basic material properties of the nanocomposites. Results are shown in table (3.5).

CNT	Amount (mass %)	Bulk Density (g/cm^3)	Young`s modulus (GPa)	Poisons ratio
	0	2.15	138	0.21
Type A	1	2.19	138	0.22
Type A	2	2.21	140	0.21
Type B	1	2.18	139	0.22
Type B	2	2.16	138	0.22

Table (3.5) Materials properties of Si-C-N cermamics incorporated with MWCNTs. [26]

SEM micrographs of the fracture surface of the type A- nanocomposite showed pulling-out and breakage of CNTs. On the other hand, in the case of the other nanocomposite, only highly distributed dark parts from the traces of CNTs are observed instead of pulled out or broken CNTs, thus indicating a deterioration of the CNTs structure in the matrix during thermolysis. According to the authors, the presence of both pulled out and broken nanotubes is due to the high strength of the embedded CNTs in combination with the well-balanced interface between CNTs and the matrix, as revealed by the presence of both pulled out and broken nanotubes.

Feng, Limeng et. al.[27] aimed to improve the strength and fracture toughness of a barium aluminosilicate (BAS) glass–glass by reinforcing it with different volume

fractions of MWNTs (from 5 to 15 vol.%). The MWNT had dimensions of 60- 100 nm in diameter and 5-15 μm in length.

After sintering the BAS/MWCNT nanocomposite at 1600 C for 1 hour, near fully dense MWNT/BAS composites were achieved except for the composite with 15 vol. % CNTs, as shown in the table (3.6). Feng et. al came to the conclusion that it is very difficult to fabricate dense glass composites with high CNT contents via a conventional powder process, because CNTs greatly inhibit the grain growth of the matrix, which is detrimental to the material densification

Materials	Relative Density (%)	Flextural Strength (MPa)	Fracture Toughness (MPa m^1/2
BAS	100	84 ± 8	1.22 ± 0.05
5 Vol. % MWNT/BAS	100	220 ± 10	2.31 ± 0.08
10 Vol. % MWNT/BAS	100	245 ± 11	2.97 ± 0.1
15 Vol. % MWNT/BAS	97	169 ± 16	2.12 ± 0.13

Table (3.6) Resultant properties of the sintered MWNT/BAS composites. [27]

Results of Feng's work show that the flexural strength of the composites increases with the increase in volume fraction of MWNTs from 5 to 10 vol.%, as shown in the figure below. The addition of 10% vol. MWNTs increases the BAS glass–glass matrix strength from 84 to 245 MPa. It indicates that the load can be effectively transferred from the BAS matrix to MWNT due to the good MWNT–BAS interfacial bonding. However, the strengthening effect of MWNTs reduces with a further increase in the MWNT volume fraction to 15%: the strength decreases from the 245 MPa recorded for the 10 vol. % MWNT/BAS composite to 169 MPa. The decrease is mainly attributed to this composite's lower relative density due to the agglomeration of CNTs.

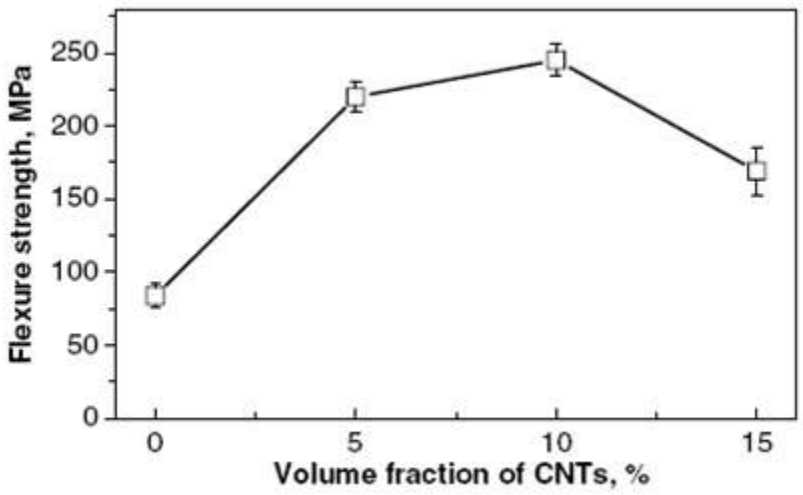

Figure (3.8) Flexural strength vs. volume fraction of CNTs, % in the MWNT/BAS composites. [27]

SEM micrographs showed that the MWNTs were homogeneously dispersed within the BAS matrix in both 5 vol. % MWNT/BAS and 10 vol. %MWNT/BAS composites, moreover, those graphs showed that there are a large number of pullout CNTs and residual holes left by CNTs, indicating the presence of an ideal CNT–BAS interfacial structure suitable for crack deflection and the pullout mechanism. The extensive crack deflection and CNTs pullout undoubtedly resulted in the increase in fracture toughness. Since the elastic modulus of the CNTs is much higher than that of the BAS matrix, the Modulus load transfer also increases toughness by transferring stresses at a crack tip to regions remote from the crack tip, hence decreasing the stress intensity at the crack tip.

The SEM micrographs in figure (3.9) show that a large number of CNTs in the wake of propagation crack bridge the two crack surfaces, which strongly support the crack bridging effect during crack propagation.

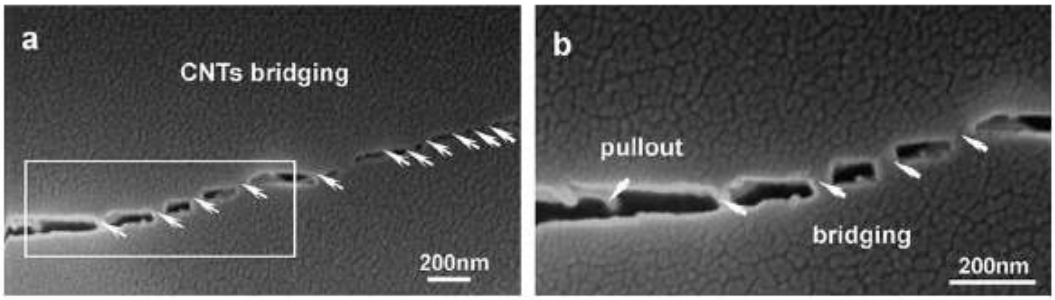

Figure (3.9) CNTs bridging and pullout in the MWNT/BAS composite. [27]

Lee and Baik et. al[43] reported that for the successful application of CNFs for the nanocomposite fabrication as a reinforcing phase, the directional control of the fiber is of great importance. The authors found that the CNFs could be aligned unidirectionally by utilizing a simple mechanical drawing process, as shown in figure (3.10a). The final composite is Cu tubing packed with CNFs. Dimensions of the dispersed CNFs are of 150 nm in diameter and 15 μm in length. SEM images of the extruded Cu pipe show fully aligned CNFs inside the tubing, as shown in figure (3.10b).

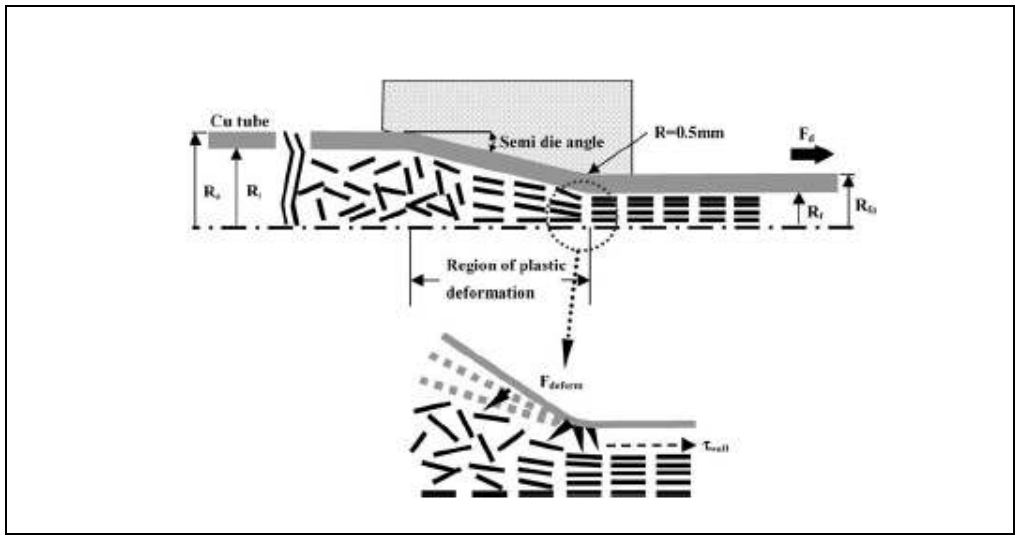

Figure (3.10a) Schematic diagram of the drawing process of the Cu tubing packed with CNFs. [43]

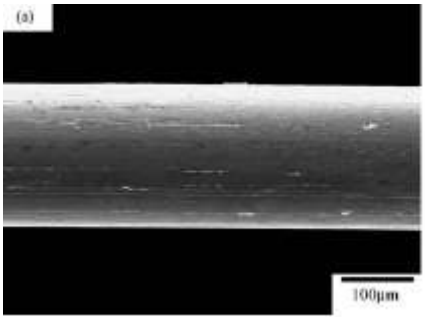

Figure (3.10b) SEM micrograph of the Cu tube packed with CNFs. [43]

In addition, Cooper and Ravich et. al[44] prepared a poly (methyl methacrylate) (PMMA) nanocomposite using a polymer extrusion technique. The lab-scale extruder was single screw with 25 mm screw diameter, and its function was to orient the nano particles in the flow direction during the extrusion process. SEM and TEM testing demonstrated the efficiency of this method for distributing and orienting the nano reinforcement materials in the polymer composite as shown in figure (3.11).

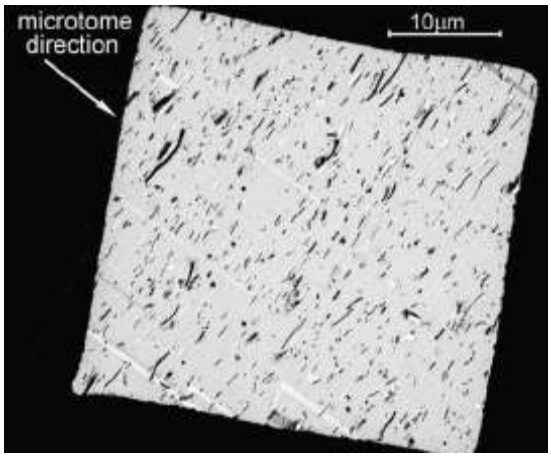

Figure (3.11) TEM micrograph of 10% wt.% nanofibrils in PMAA. [44]

As the literature search reveals, there has been no work associated with adding nano materials to glass during the glass fiber drawing process. The new method of imbedding, dispersing and aligning the CNFs in the glass matrix will resolve all the issues that are related to the reinforcement of glass fibers.

3.4 CNTs versus BNNTs

Recently, some scientists have asserted that Boron Nitride nanotubes have some important advantages over Carbon nanotubes[28]. For example: BNNTs are far more resistant to oxidation than CNTs and therefore suited for high-temperature applications in which carbon nanostructures would burn, in addition, BN nanotubes are expected to be semiconducting, with predictable electronic properties that are independent of tube diameter and number of layers, unlike CNTs, moreover, BNNTs are more stable at higher temperatures. However, low hardness and strength, inadequate abrasion resistance in a high velocity stream, and limited corrosion

resistance above 1000°C in an oxidizing atmosphere, reduce the possibilities for utilizing BNNTs[29].

Its been shown that boron nitride relates to a number of materials that are most difficult to sinter and in order to achieve with hot pressing a density of 2.0- 2.2 g/cm3 (88-97% of the theoretical density) considerable energy expenditure, and the use of sintering activators and preliminary powder preparation (annealing, explosive treatment) are necessary.[30]

Masa, Shaul et. al.[31] pointed out that structures of graphite nanotubes and hexagonal boron nitride nanotubes (h-BN), basic materials for carbon nanotubes and boron nitride nanotubes are quite similar. Figure (3.16) compares their structures. They are both layered materials composed of layers of hexagonal lattices; graphite has carbon atoms at all lattice points, while h-BN is composed of alternating atoms of boron and nitrogen.

One minor difference between these materials is in their layer stacking. In h-BN, layers are arranged so that boron atoms in one layer are located directly on top of nitrogen atoms in neighboring layers and vise versa. As shown in Figure (3.16a), the hexagons lie on top of each other. In graphite, the stacking is slightly different; hexagons are offset and do not lie on top of each other. The following table gives a general comparison between CNT`s and BNNs.

	CNT	BNNT
Electrical Properties	Metallic or semiconducting	Always semiconducting
Young`s Modulus	1.33 TPa	1.18 TPa
Thermal Conductivity	> 3000 W/mk	600 W/mk
Chemical Resistance	Stable up to 300- 400 C	Stable up to 800 C

Table (3.7) Comparison of properties of CNTs and BNNTs. [31]

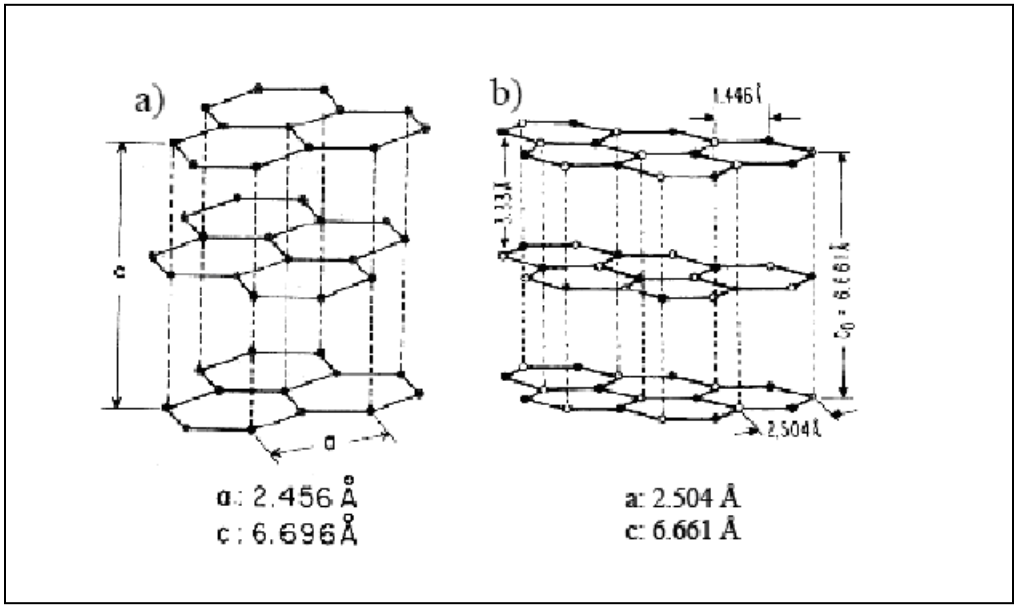

Figure (3.12) Structure of parent materials: a) Graphite
b) Boron Nitride

Janet Hurst et al.[32] studied the effect of adding Barium calcium aluminosilicate glass composites (G18) to ~4% by weight of BN nanotubes with diameters of 10 to 40 nm and lengths of tens of microns. The new reinforced composite was fabricated by hot pressing.

The strength and fracture toughness of the composite were higher by as much as 90 and 35 percent, respectively, than those of the unreinforced glass. Hurst reported that the addition of just 4 wt.% BN nanotubes increases the glass strength from 48 ± 7 MPa to 92 ± 17 MPa. This 90 percent increase in strength of the glass with BN nanotube reinforcement is notable, compared with a moderate strength increase (40 to 60 percent) for G18 glass reinforced with 5 mol% alumina platelets or zirconia particulates. These results are shown in figure (3.17).

As for the fracture toughness, the results show similar trend as strength. However, the increase in fracture toughness was less significant than strength. Moreover, the addition of just 4 wt.% BN nanotubes increases the fracture toughness (*K*Ic) of glass from 0.51 ± 0.03 MPa√m to 0.69 ± 0.09 MPa√m. This 35 percent increase in fracture toughness for the glass-BN nanotubes composite is comparable to that for the G18 glass composites reinforced with similar amounts of alumina or zirconia.

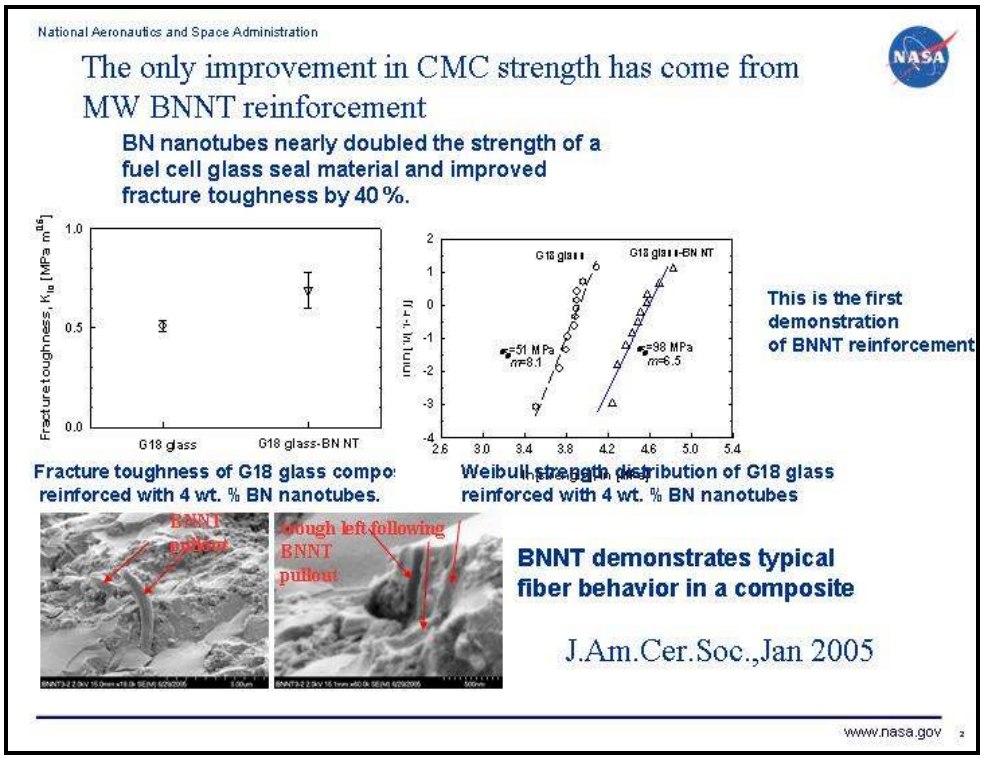

Figure (3.13) Boron Nitride reinforced glass matrix. [32]

CHAPTER IV

ANALYTICAL ANALYSIS AND MODELING

4.1 Introduction

The tensile strength of a material is the maximum amount of tensile stress that it can be subjected to before failure. The definition of failure can vary according to the material type and the design methodology. A graphical description of the amount of deflection under load for a given material is the stress-strain curve. The yield stress, ultimate tensile stress, and elastic or Youngs modulus of a material can all be determined from the stress-strain curves. At small strain values (the elastic region), the relationship between stress and strain is nearly linear. Within this region, the slope of the stress-strain curve is defined as the elastic modulus. The point at which this line intersects the curve is called the yield point or the yield stress.

Stresses on the fiber can be calculated using the formula:

$$\text{Stress } (\sigma) = \text{Force/cross sectional area} \qquad (Pa)$$

$$\sigma = 4P/\pi \times D^2 \tag{4.1}$$

And the accompanied strain is:

$$\varepsilon = \Delta L/L_0 \tag{4.2}$$

Where:

P: Applied Force (N)

D: Fiber Diameter (μm)

L_0: Initial length of the fiber sample (mm).

ΔL: Change in fiber length before and after the test (mm).

Modulus of elasticity can be calculated using the equation:

$$E = \frac{\sigma}{\varepsilon} \tag{4.3}$$

Where E is the modulus of elasticity (MPa), σ is the ultimate stress (MPa) and ε is the strain (%)

4.2 Tensile Strength Modeling

The ultimate tensile strength properties of fiber-reinforced glass matrix composites are usually dictated by the strength of the fibers. The fibers exhibit a statistical variation of strength that obeys a two-parameter Weibull law. Provided the fibers are subjected to global load sharing, the load transmitted from each failed fiber

is shared equally among the intact fibers, the fiber volume fraction V_f is related to the ultimate tensile strength σ_{UTS} as[52]:

$$V_f = \frac{\sigma_{UTS} x R_f}{L_o x \tau x F(m)} \tag{4.4}$$

Where R_f is the reinforcement fiber radius (μm), τ is interfacial shear resistance (MPa), and the function F depends upon the shape parameter (m) and it's given by:

$$F(m) = \left(\frac{2}{m+2}\right)^{1/(m+1)} \frac{m+1}{m+2} \tag{4.5}$$

A simple and effective way to predict the properties of fiber-reinforced composites, given the component properties and fiber volume fraction, is the rule of mixtures (ROM). A basic concept in the ROM method is the evaluation of each contribution of the fiber and the matrix at the point of failure, and calculation of the ultimate strength of the composite as the sum of contributions according to their relative volumetric properties.

The ROM method is states that:

$$\sigma_{com} = \sigma_m (1 - V_f) + \sigma_f (V_f) \tag{4.6}$$

Where:

σ_{com} is the overall composite tensile strength (MPa), σ_m is the matrix tensile strength (MPa), , V_f is the fiber volume fraction (%), and σ_f is the carbon nanofiber tensile strength (MPa).

While the ROM indicates that the strength of a composite increases linearly as the fiber volume fraction increases, the strength of a real composite deviates from the ROM in a non-linear fashion and usually begins to decrease above a fiber volume fraction of 80%.

All the tensile strength modeling for nanocomposite materials that has been developed so far assume that the imbedded reinforcement materials are continuous and uniform, however, this is not the case when CNTs or CNFs are used as reinforcement materials. The models mentioned in section (4.2) only provide us with a rough estimate of the CNF/glass frit nanocomposite fibers tensile strength.

4.3 Post Cracking Modeling

The post-cracking behavior of short-fiber reinforced brittle-matrix composites can be predicted by the use of a composite bridging stress-crack opening displacement (σc- δ) relationship. The (σc- δ) relationship describes the constitutive relationship between the traction (σc) acting across a matrix crack plane and the separation distance (δ) of the crack faces in a singly pre-cracked uniaxial tensile specimen loaded to complete failure.

A mathematical model for predicting the complete (σc- δ) relationship is derived for a brittle-matrix reinforced with short, randomly distributed fibers having a tensile strength distribution satisfying the Weibull's weakest link statistics.

When a crack propagates perpendicularly to the fibers in unidirectional fiber - reinforced ceramics with a weak fiber /matrix interface, fiber debond from the matrix and slip over a certain distance. Consider a single fiber bridging a plane crack as

shown in Figure (4.1). Following a shear-lag analysis, Li and Leung[34] developed a relationship between length *y* and the stress in the fiber σ_d:

$$\sigma_d = \frac{4\tau(1+\eta)}{d_f} y \tag{4.7}$$

Where:

σ_d : Stresses in the fiber (*MPa*)

τ : Fiber/Matrix shear stress (*MPa*)

$\eta = \frac{V_f E_f}{V_m E_m}$, V_f : Volume fraction of the fiber

E_f : Young`s modulus of the fiber (*MPa*)

V_m : Volume fraction of the matrix

E_m : Young`s modulus of the matrix (*MPa*)

d_f : Fiber diameter (*mm*)

y : Deponding length of the fiber (*mm*).

Equation (6.1) yields:

$$y = \frac{d_f}{4\tau(1+\eta)} \sigma_d = \lambda \sigma_d \tag{4.8}$$

Where: $$\lambda = \frac{d_f}{4\tau(1+\eta)}$$

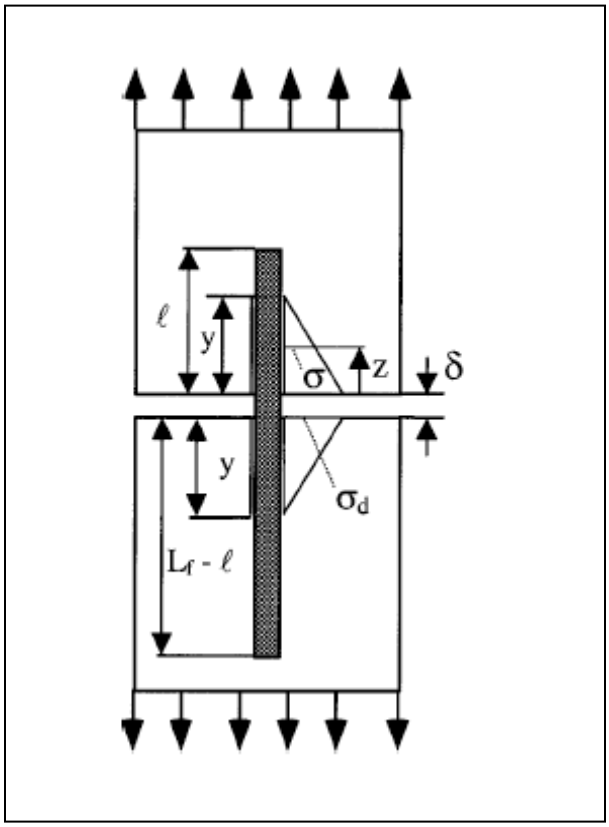

Figure (4.1) Single fiber bridging a plane crack

In Li and Leung[34] model, debonding was interpreted as the activation of a frictional bond stress τ between the fiber and the matrix. In addition, they derived a fiber stress displacement relationship:

$$\sigma_d = \sqrt{\frac{4\tau(1+\eta)E_f\delta}{d_f}} = \frac{L_f}{2\lambda_e}\left(\frac{\hat{\delta}}{\hat{\delta}^*}\right)^{1/2} \qquad \text{for } 0 \le \delta \le \delta_o \qquad (4.9)$$

and the fiber pullout stress:

$$\sigma_p = \frac{4\tau(l + \delta_o - \delta)}{d_f} \qquad \text{for } \delta_o \le \delta \le l \qquad (4.10)$$

Where:

δ: Crack opening displacement (*mm*)

$$\hat{\delta}^* = \frac{2\tau L_f}{(1+\eta)E_f d_f} \quad , \qquad \hat{\delta} = \frac{\delta}{(L_f/2)}$$

and

$$\delta_o = \frac{4\tau l^2}{(1+\eta)E_f d_f}$$

Based on weakest link statistics, Thoulas and Evans[35] derived a probability density function for fiber failure as a function of the peak stress σ_d and the distance from the crack zone z:

$$\phi(\sigma_d, z) = \frac{m(m+1)}{2\lambda S^{m+1}} \exp\left[-\left(\frac{\sigma_d}{S}\right)^{m+1}\right] \times (\sigma_d - \frac{z}{\lambda})^{m+1} \qquad (4.11)$$

Where:

m: Weibull modulus (shape parameter)

$$S = \left[\frac{S_o^m (1+m)}{2\pi d_f \lambda} \right]^{\frac{1}{1+m}}$$

In which: S_o: Scale parameter= $\sigma_o A_o^{1/m}$, A_0 is the fiber unit surface area ($=\pi d_f L_0$).

The failure probability of fibers having an embedment length l is given by:

$$q_f(l) = 2\int_0^{\frac{l}{\lambda_e}} \int_0^{y=\lambda\sigma_d} \phi(\sigma_d, z) dz d\sigma_d \qquad (4.12)$$

The factor 2 used in equation (6.6) accounts for the fact that fibers could fail on either side of the crack, and therefore, both sides of the crack must be considered.

4.4 CNFs Alignment Modeling

Aligning CNFs in composites has been one of the most important issues in the nanocomposite area that many researchers are exploring. Several methods, including centrifugal forces and electrical fields, have been attempted to cause unidirectional alignment of fibers[42]. Recently, other new techniques have been implemented that utilizes a drawing or an extrusion process to align the CNFs in the preferred direction.

According to Nayfeh and Hurst[51], the alignment of the nano materials in the flowing glass during the glass fibers forming process will obey fluid dynamics laws by taking advantage of the shear forces, that are acting on the nano materials surfaces, to align the materials in the direction of flow, as long as the flow is laminar.

Fluid dynamics states that the flow of fluids exhibit viscous effects, that is they tend to stick to solid surfaces and have stresses within their body. This phenomenon can be expressed by Newton's law as[45]:

$$\tau = \mu\,(du/dy) \qquad (4.13)$$

Where:

τ : Shear Stress (Pa)

μ: Viscosity (Pa.s)

du/dy : change in velocity with y direction (1/s)

Since fluids are viscous, energy is lost during flowing by friction. The effect of friction is usually shown as pressure or head loss. At the wall surface of a pipe with fluid flowing inside, shear stress will develop and retard the flow. Assuming that the flow is laminar, the velocity profile is parabolic of the form $y=ax^2 + b$. This is shown in figure (4.2).

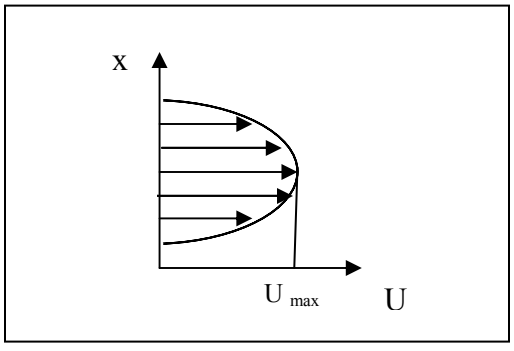

Figure (4.2) Velocity profile for a viscous material flowing in a pipe

If we consider a flowing filament, as shown in figure (4.3), the pressure at the upstream is p, and the pressure at downstream will fall by Δp to (p-Δp).

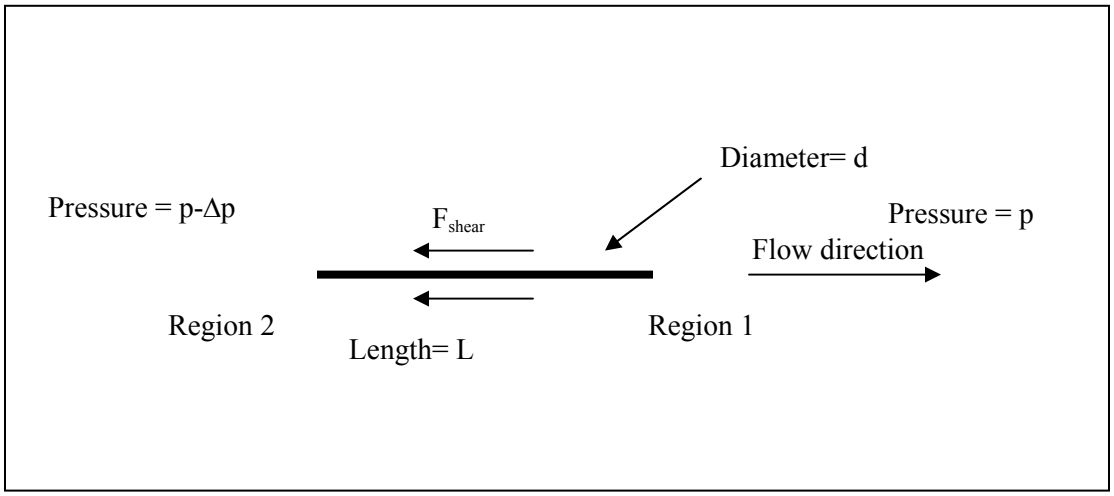

Figure (4.3) Cylindrical element of length L flowing in the direction of flow

Forces acting on a cylindrical element of diameter d and length L can be divided into:

The driving force due to the pressure difference (F = Pressure × Area), this force can be expressed as:

F_{drive} = driving force = Pressure force at region 1 - pressure force at region 2

$= pA - (p-\Delta p)A$

$= \Delta p \times A$

$= \Delta p \, (\pi d^2/4)$ (4.14)

2. The retarding force due to the shear stress:

F_{shear} = shear stress × area over which it acts

$= \tau_w \times$ area of cylinder wall

$= \tau_w \pi d.L$ (4.15)

In case the filament is flowing with an angle θ from vertical, the drive force as well as the shear force will act on the filament as shown in figure (4.4).

M is the moment generated due to F_{drive}.

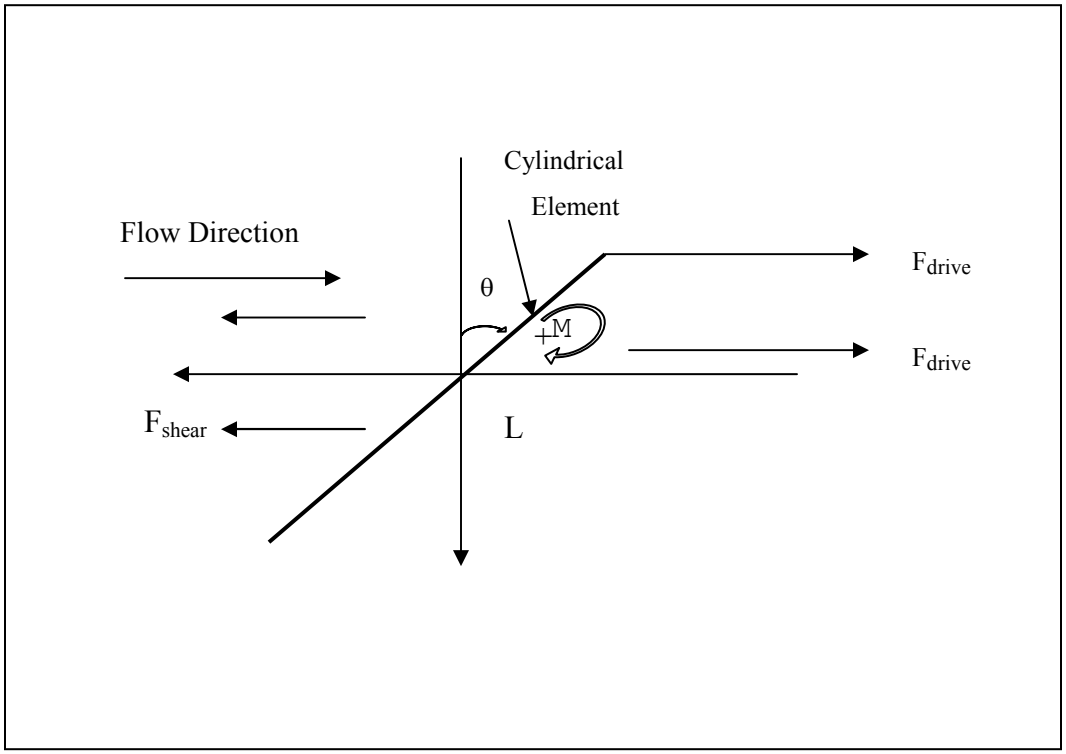

Figure (4.4) Element flowing with an angle θ

The element will move in the direction of flow as long as $F_{drive} > F_{shear}$ $sin\theta$. Moreover, to minimize resistance, the moment M given in equation (4.14) will force the element to rotate around its axis to reach the equilibrium state at which M is equal to zero. Equating equation (4.15) to zero yields a value of θ equals to

90^0, which means that the element at this point is flowing parallel to the direction of flow, as shown in figure (4.5).

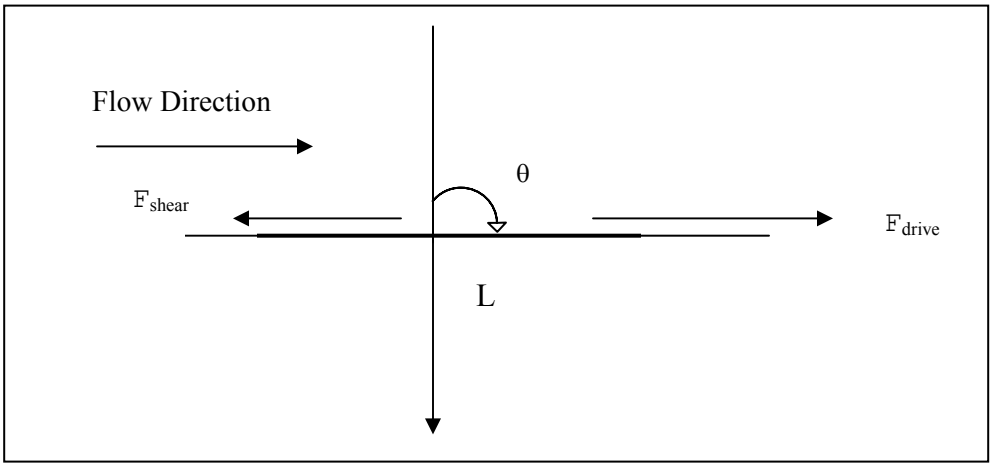

Figure (4.5) Element flowing at $\theta = 90^0$

The angular velocity for the rotating filament was given by Suciu et al[39]. as:

$$\omega(\theta) = \frac{F_{shear}}{\zeta_{friction}} \sin\theta = \frac{\tau_w . A}{L^6 \eta_s} \sin\theta \qquad (4.16)$$

Where $\zeta_{friction}$ is coefficient of friction, η_s is the viscosity of the fluid phase

Nayfeh and Hurst[51] stated that the carbon nanofibers will behave in a very similar manner to the above phenomenon, where shear forces generated during the glass drawing process will align the CNFs in the direction of the flowing glass.

CHAPTER V

EXPERIMENTAL WORK AND PROCEDURES

5.1 Introduction

The development of the hybrid E-glass fibers/CNFs composite was carried out in three main experiments: The first experiment was a feasibility study at which the preliminary results were obtained. This experiment involved using encapsulated CNF's coupons at 20% by weight concentration mixed non-uniformly with 18 Kg (40 Ibs) of E-glass marbles. The second experiment is the intermediate experiment and it was a replication of the first one. In this experiment, three coupons (total mass 38 g) at 20% wt. CNFs were dropped inside the premelter of the glass-drawing tower. The premelter contained 18 Kg of molten E-glass. The third experiment was carried out using E-glass frit that was prepared in our lab and mixed with 5% wt. CNFs.

The glass fiber-drawing machine at Cleveland State University was used to produce the continuous E-glass/CNFs nanocomposite fibers. The machine has two operational modes depending on the desired glass fiber diameter. The first mode involves wounding continuous lengths of glass fibers 7-20 μm in diameter using the winder that rotates at different speeds, with a minimum speed of 1200 RPM. The second mode is used to produce thicker glass fiber, 20 to 90 μm in diameter, using the pull rolls.

The machine has a 90/10 Platinum/Rhodium furnace, known as the premelter. The premelter can hold up to 18 Kg (40 Ibs) of glass marbles. The E glass melting temperature is 1200^0 C. Solid E glass marbles of different formulations is the input material in the process. The molten glass is gravity fed to a Platinum bushing with 198 tips each 1.8 mm in diameter (drawing speed is what ultimately determines the fiber diameter) and 5.07 mm in length. The tips are arranged in 11 rows and 18 columns. As glass filaments flow out of the tips, they are cooled and attenuated to their final desired diameter, lubricated, gathered into one strand and wound onto a winder. The process is shown in figure (5.1).

The feedstock preparation is presented hereafter followed by a brief description of the pull test machine. Finally, the experimental work and procedures are presented at the end of this chapter.

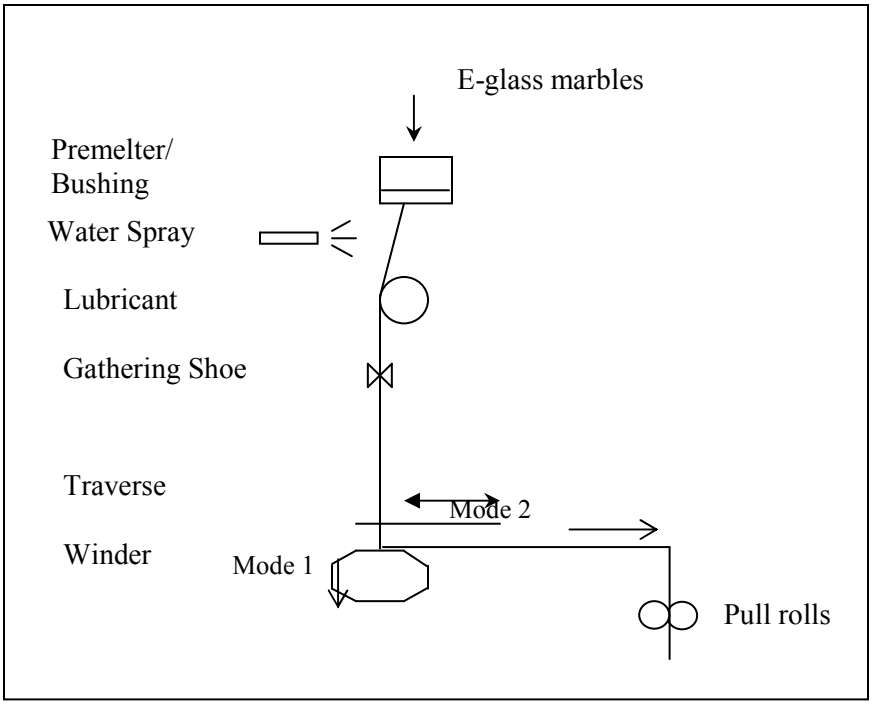

Figure (5.1) Schematic of glass fiber drawing machine

5.2 Feedstock Preparation

5.2.1 Carbon Nanofibers (CNFs)

The multi-wall carbon nanofibers (CNFs) used in our experiments were supplied by Applied Sciences Inc. (Product name: PR24LHT). CNFs were heat treated at 1500 ^{o}C to improve their tensile strength. The following is their nominal properties after the heat treatment:

Mean Diameter	100-200 nm
Mean Length	200-300 μm
Tensile Strength	7-15 GPa
Tensile Modulus	600 GPa
Density	1.2 g/cm^3
Optical Properties	Black none fluorescent in bulk
Electrical Resistively	55 Microohm/cm
Thermal Conductivity	1950 W/m-k

Table (5.1) CNF properties for the conducted experiment

5.2.2 E-glass Frit

E-glass frit was used during the third experiment. The glass frit was first produced by pulling glass fibers without applying a lubricant or a sizing material on the fibers surface. The fibers were then washed by water to remove any contaminations on the surface. A sharp blade was used to chop the fibers into small pieces, about 1 to 3 inches long. The chopped fibers were then wet blended in water using a commercial high speed-high power blender. Finally, the glass frit was dried in a conventional oven at 100 ^{o}C. The produced frit shown in figure (5.2) had a mean length of about (450μm). Figure (5.3) illustrates the process of producing the glass frit.

Figure (5.2) Glass frit

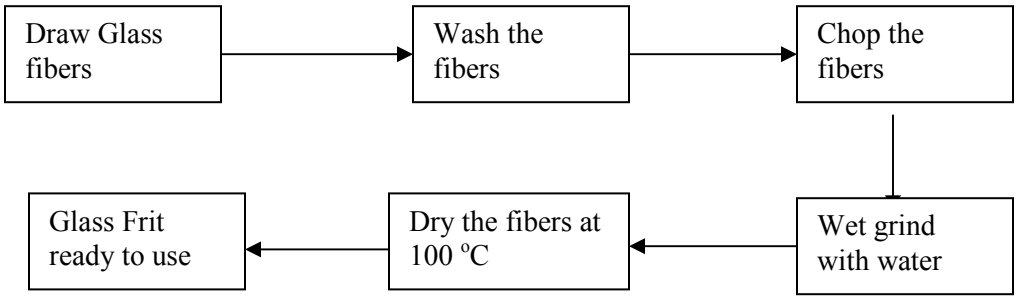

Figure (5.3) Glass Frit Production Procedures

5.2.3 E-glass Frit/CNFs Mix

Mixing the E-glass frit with the CNF's was carried out in a stainless-steel jar that was placed on top of a jar mill that is shown in figure (5.4) (manufactured by: U.S Stoneware). The jar was filled with both the CNF's and the glass frit. Acetone

was added to the mix to help disperse the CNF's in the glass frit during the tumbling. Few glass marbles were also added to prevent agglomeration of the CNF's during the mixing process. The mixture was tumbled for 24 hours for each batch. After the tumbling is over, the mix was exposed to air to let dry for 4 hours before using it. Figure (5.5) illustrates the process of mixing the glass frit with the CNF's.

Figure (5.4) Jar mill used to tumble CNFs/glass frit mix

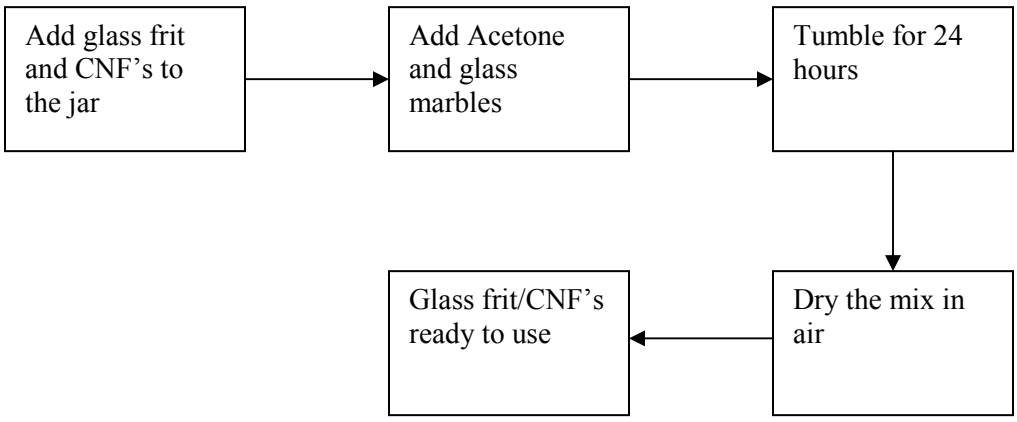

Figure (5.5) Glass Frit/CNF's mixing procedures

5.3 Tensile Strength Machine

A tabletop tensile strength machine was used to measure the strength of the glass fibers. The machine is manufactured by ADMET (model: eXpert 5606). Figure (5.6) shows the machine.

The pull test was conducted using a 1 KN load cell at 0.05 min^{-1} strain rate. Pressurized air at 50 psi was used to provide the necessary gripping force on the grippers and hence on the fibers. The machine is equipped with software that's capable of giving online readings for the applied load and the corresponding displacement.

Figure (5.6) Tensile strength machine (ADMET)

To obtain the maximum accuracy during the fibers testing, small and light weighted grippers were used to avoid the effect of the weight of the grippers on the tensile strength measurements.

Fibers produced by dropping the encapsulated CNF's coupons (first and second experiments) were tested using the fiber bundle technique. This technique was used due the fact that the drawn fiber filaments were small in diameter (12 μm), which makes it hard to carry out a single fiber test.

Performing a fiber bundle tensile test is, sometimes, more advantageous than the single fiber test. For example, the single fiber test is not only more difficult to conduct, but also may not produce meaningful information on the failure of fibers in an actual composite material. The principal reason for this is that single fibers are not used in composites; instead, they are bundled together for easier processing and handling. In the bundle form, the breakage of one fiber or a group of fibers does not lead to an immediate failure of the bundle, since the remaining fibers in the bundle can still carry the load.

In a fiber bundle test, the static tensile strength distribution of single fibers is determined from the measurement of tensile strength distribution of fiber bundles. The fiber bundle model is shown in figure (5.7). In this model, a fiber bundle, initially containing N parallel fibers, each of length L and cross-sectional area A, is rigidly fixed at both ends by an adhesive material, product name: 5 minute Epoxy Gel.

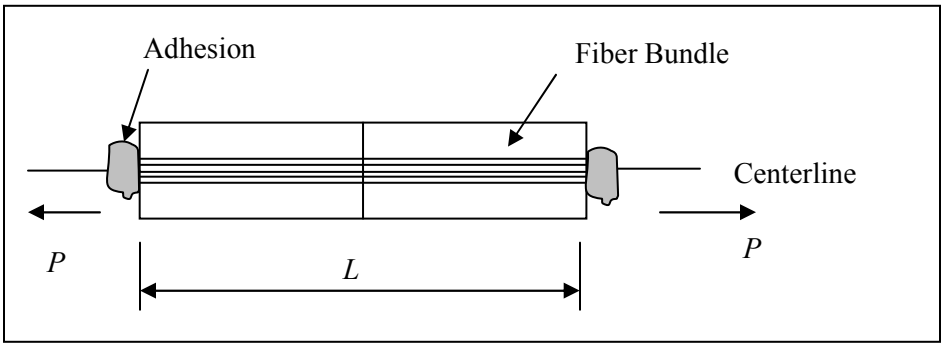

Figure (5.7) Schematic diagram of the fiber bundle specimen

Fibers produced by mixing E-glass frit with CNF's (the third experiment) were relatively thick, about 50 μm in diameter, and hence, they were suitable for performing a single fiber tensile test. The test setup is similar to the fiber bundle one and it is shown in figure (5.8).

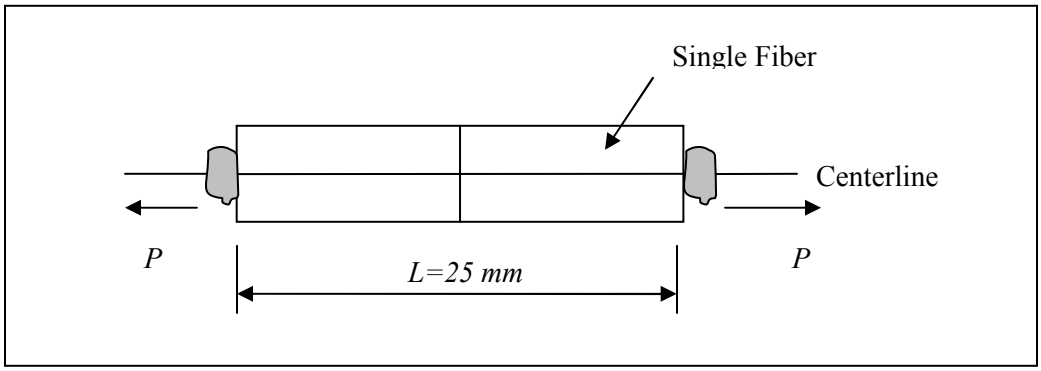

Figure (5.8) Schematic diagram of the single fiber specimen

5.4 Experimental Procedures

5.4.1 First Experiment: E-Glass/Encapsulated CNFs Coupon

In the preliminary experiment, a 20g E-glass/CNF coupon containing 20% wt. carbon nanofibers was dropped in the center of the premelter of the glass drawing tower. The premelter contained 18 Kg (40 lbs) of undistributed E glass melt. Due to the differences in the specific gravities between the coupons and the pure E glass, and the lack of agitation, the carbon nanofibers didn't mix uniformly with the undistributed glass in the melter. The experiment was not controlled in that the ultimate concentration of the carbon nanofibers in the glass filaments is not known. The experiment setup is shown in figure (5.9).

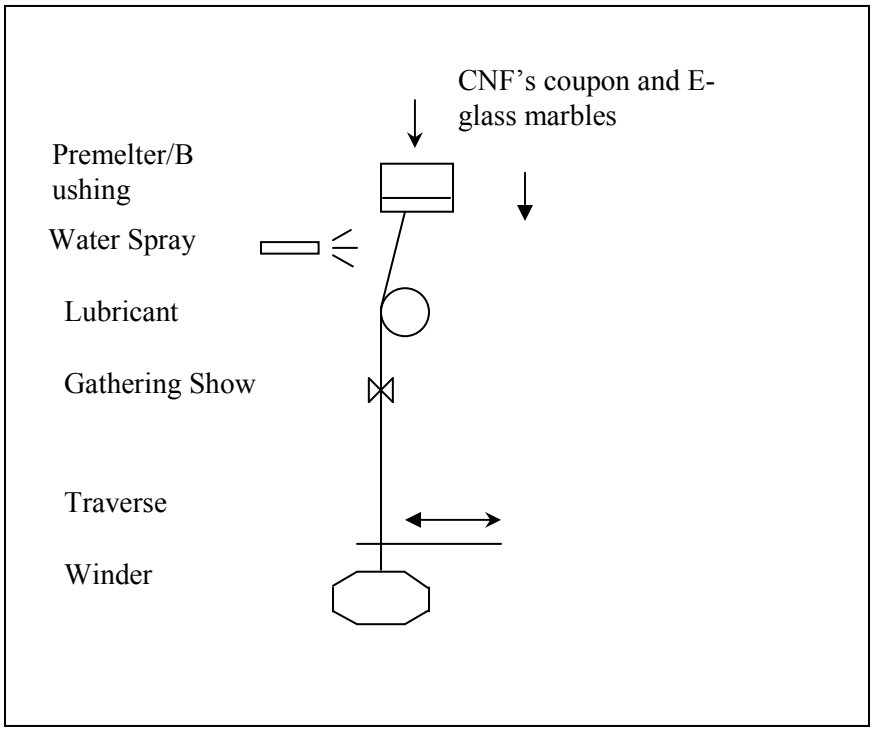

Figure (5.9) First experiment setup

The drawn filaments were continuous and their diameters were on the order of 30-40 μm. It is estimated that in the best-case scenario, the concentration of the carbon nanofibers in the glass filaments was fairly small perhaps on the order of 1%-2% by vol. The areas of the filaments containing the carbon nanofibers fluoresced in gold when exposed to UV long wavelength (354 nm) light. Optical tests conducted on the bulk CNT material have shown a lack of florescence in the visible.

5.4.2 Second Experiment: E-Glass/Encapsulated CNFs Coupons

The second experiment involved using three coupons of encapsulated CNF's and E-glass with a total of 38 g at 20% wt. CNF's. The coupons, that were prepared at NASA Glenn by hot pressing in vacuum, were crushed into small pieces before dropping them in the middle opening of the premelter. The premelter was then covered by a layer of E-glass marbles to protect the CNF's from oxidation

The idle time, which is the time required to reduce the air bubbles in the molten mixture, was about 45 minutes. Figure (5.10) shows the experiment setup. The drawn and wound glass filaments were 12 μm in diameter and exhibited the gold color when exposed to a long wave UV light.

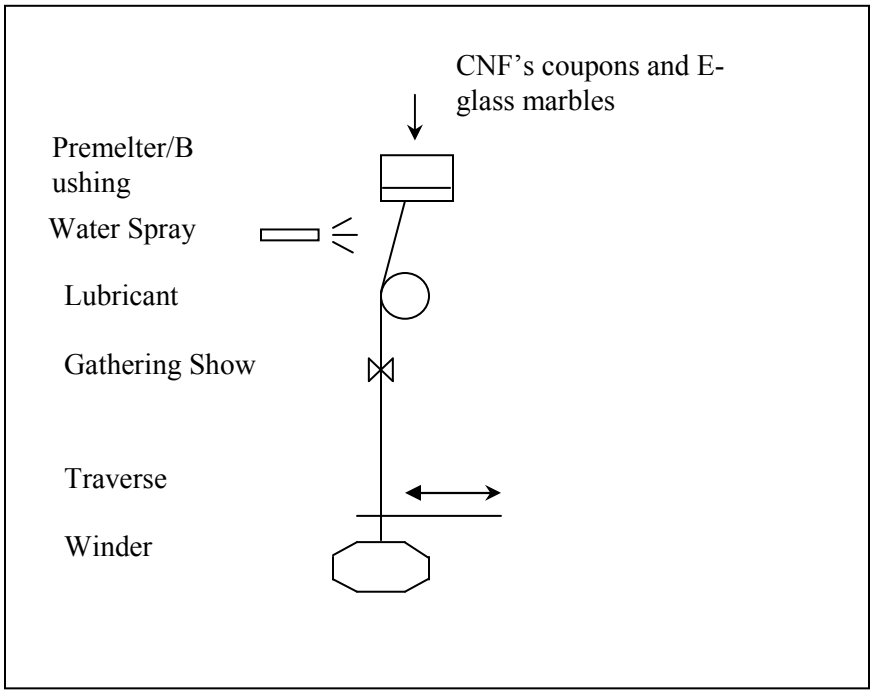

Figure (5.10) Second experiment setup

5.4.3 Third Experiment: Glass Frit/CNFs Mix

The third experiment produced fibers by mixing E-glass frit with 5% wt. CNF's as feedstock material. The experiment setup is shown in figure (5.11). To protect the screen inside the premelter from overheating and causing damage to it, glass frit/CNFs mix was added to the premelter after dropping the glass level to 1 inch above the screen. A frit feeding mechanism and a Nitrogen purging system were setup next to the hopper of the glass-drawing machine.

The frit feeding mechanism (shown in figure (5.12)) was used to feed the glass frit mix into the premelter through a stainless steel tube. The system consisted of a variable speed DC screw feeder, a hopper and stainless steel tubing. The screw

feeder is connected to the hopper, that holds the CNF's/glass frit, from one end and to the premelter, through the stainless steel tubing, from the other end. To prevent oxidization of the CNF's in the premelter, Nitrogen was purged inside the feeder hopper as well as inside the premelter through a Nitrogen piping system that was built for that purpose.

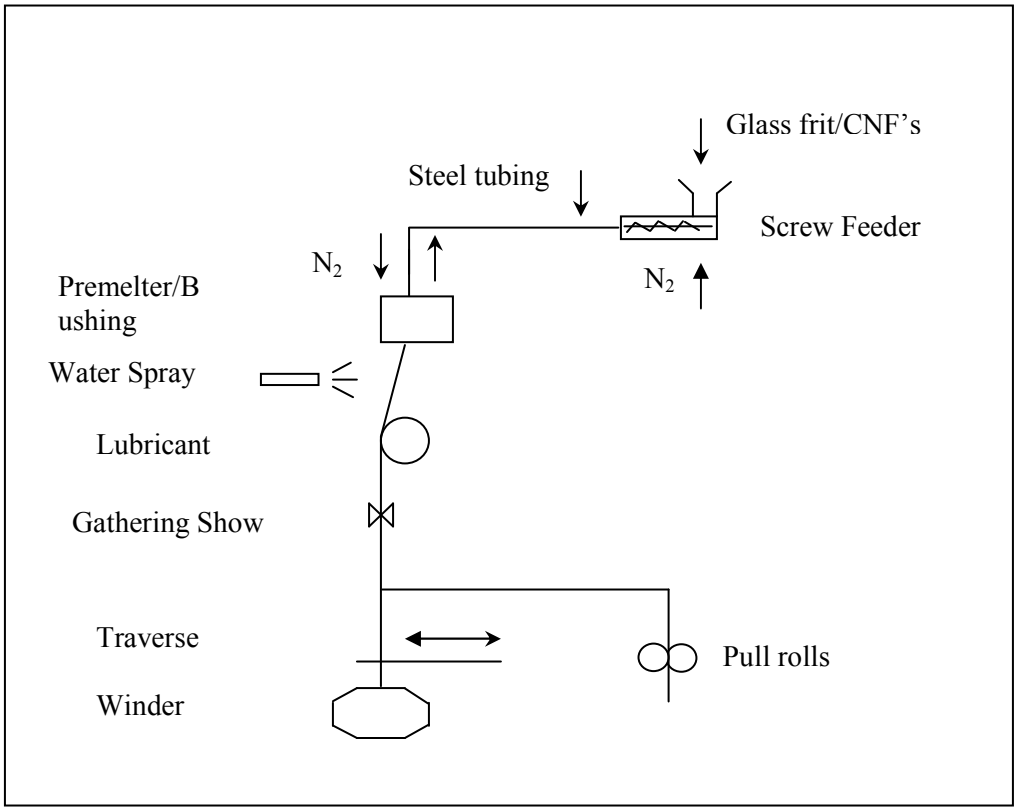

Figure (5.11) Third experiment

Figure (5.12) CNFs/glass frit feeder

Fibers were pulled out on 12 runs, each run lasted for 5 minutes; with a mean filament diameter of about 50 μm.

CHAPTER VI

RESULTS AND ANALYSIS

6.1 Introduction

Results obtained from the three experiments are presented hereafter. Tensile strength tests as well as optical tests were performed on the selected samples from each experiment. The obtained results confirmed that the CNFs survived the high temperatures during the glass fiber forming process, in addition for being well dispersed and aligned in the glass fibers. As a result, the imbedded CNFs increased the strength of the glass fibers significantly.

6.2 First Experiment: E-Glass/Encapsulated CNFs Coupon

Early analysis of the fibers produced during the first experiment indicated that the CNFs were well dispersed and aligned during the drawing process along with the axis of the E glass filaments as shown in figure (6.1).

Pull tests were conducted on a population of 20 tows of fibers each containing approximately 200 filaments. The tests indicated that there is a significant increase in the tensile strength of the fibers containing the CNFs (% of CNFs is low and unknown). The results of the pull tests are displayed in figure (6.2) and indicate that the strength of the fibers increased by nearly 50% and in some cases doubled.

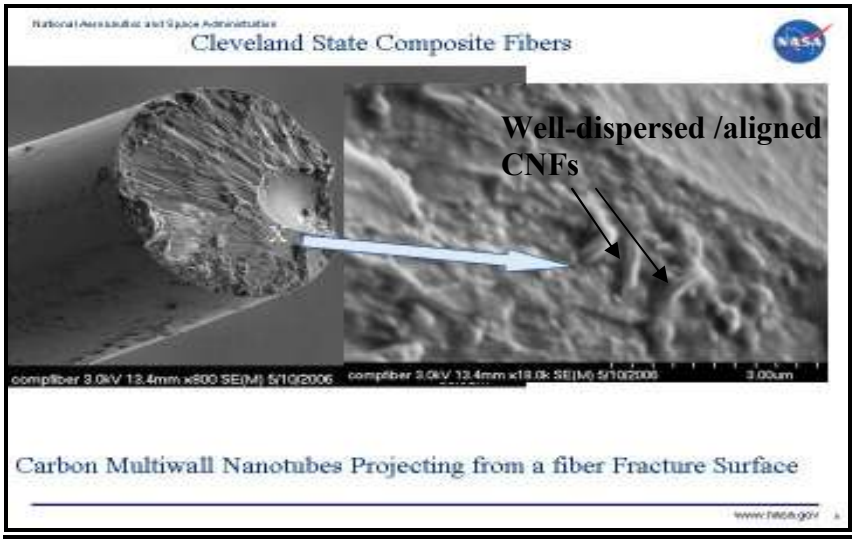

Figure (6.1) Well dispersed CNTs in the strong composite fiber [Source: Janet Hurst, NASA -GRC]

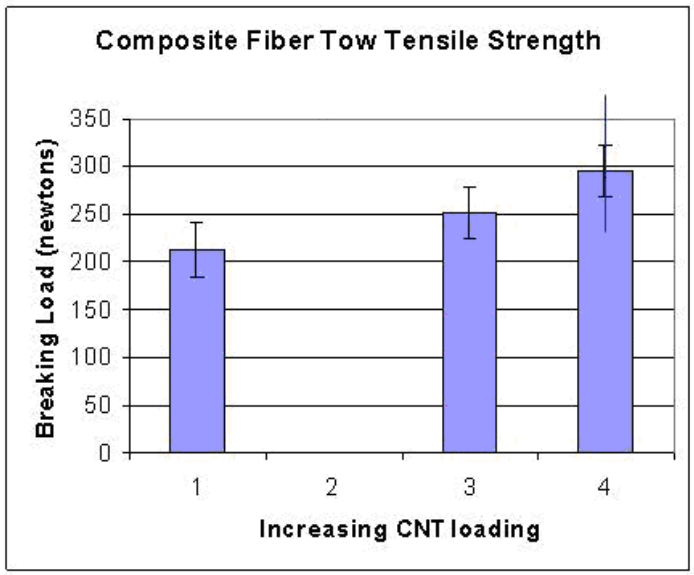

Figure (6.2) Breaking load results for the conducted experiment [Source: Janet Hurst, NASA -GRC]

The fracture surfaces of the hybrid fibers were considerably different from that exhibited by normal E glass fibers. Figure (6.3) shows that the brittle fracture surface shown on the left in the image is considerably modified to a semi ductile fracture due to the presence of the CNFs in the fibers on the right.

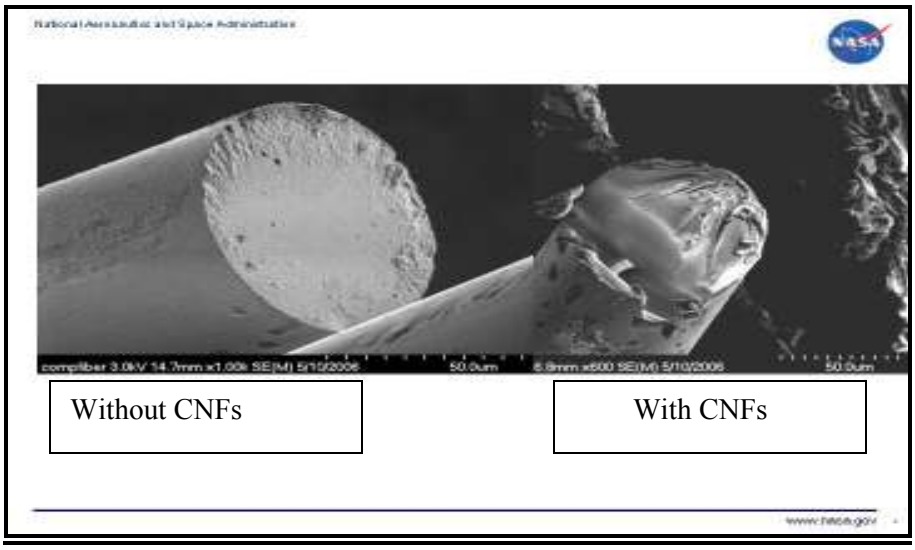

Figure (6.3) Fracture surfaces of the E glass filaments with and without CNFs [Source: Janet Hurst, NASA -GRC]

6.3 Second Experiment: E-Glass/Encapsulated CNFs Coupons

Samples from fibers produced during the second experiment were tested to determine their tensile strength. A population of 250 tows, each containing 198 filaments, was tested. Virgin glass samples were also tested for comparison purposes. A population of 100 samples of virgin glass was tested for their tensile strength.

Fibers in this experiment gained significant increase in their tensile strength of about 60%, compared to the virgin glass strength, as shown in figure (6.4). It is certain that some samples contained very little CNFs in the glass matrix. This can be verified in the samples having a tensile strength values close to the ones of virgin

glass strength values. In the best-case scenario, the tensile strength for those fibers was about 6 GPa, which is two times stronger than pristine E-glass fibers that have a tensile strength value of 3.3 GPa.

This experiment confirmed the results obtained in experiment 1 that adding CNF's to E-glass during the drawing process will indeed increase the strength of the fibers significantly.

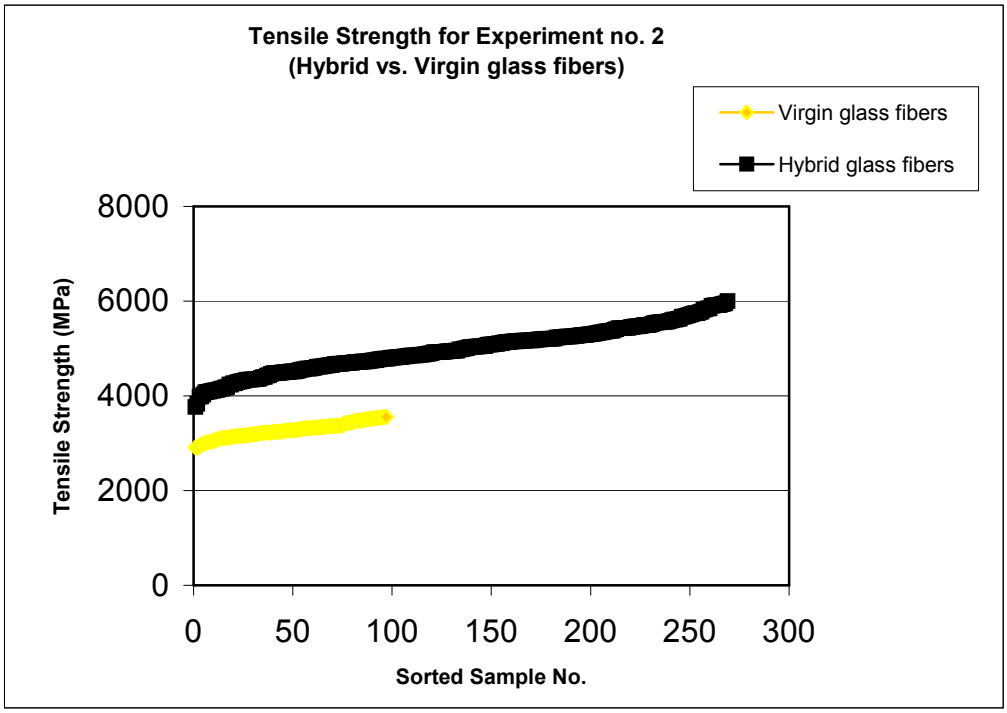

Figure (6.4) Results obtained for the second

The histogram plot of tensile strength for the virgin glass as well as the hybrid fibers is shown in figure (6.5). The plot shows two separate populations of glass fibers. The wide range of the tensile strength distribution for hybrid fibers is mainly caused by poor mixing of the nano fibers in the glass during the glass drawing, which causes a non-uniform distribution of CNFs in the glass matrix.

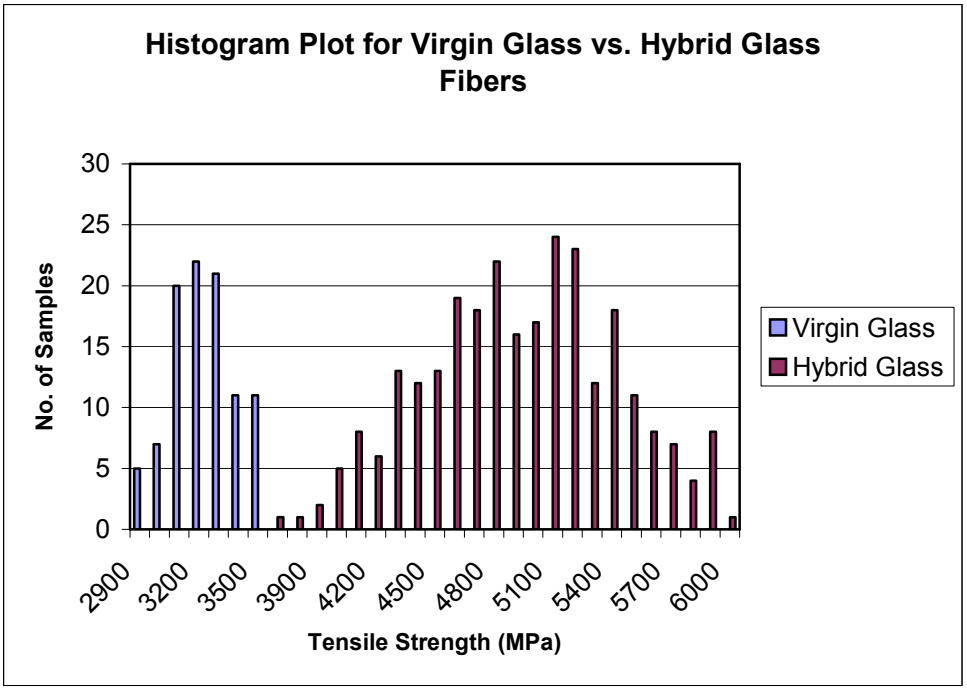

Figure (6.5) Histogram plot for experiment 2

6.4 Third Experiment: Glass Frit/CNFs Mix

In the third experiment, fibers were drawn throughout 12 runs, each run lasted for 5 minutes. The fibers were continuous and their mean diameter is 50 μm.

Fibers from Run 1 through Run 12 were tested for their tensile strength properties. A population of 270 samples from run 1 and 400 samples from run 2 were randomly selected and tested. Tables (6.1) and (6.2) show a statistical summary of breaking loads for the tested fibers from runs 1 and 2.

Test number	No. of tested samples	Mean (N)	Max (N)	Min (N)	Median	Fiber diameter (μm)
1	19	12.15	18.13	3.98	12.56	50
2	28	10.33	17.09	6.1	9.17	50
3	24	10.38	15.84	5.37	9.67	50
4	32	10.82	19.22	6.23	9.93	50
5	56	9.08	14.32	5.22	8.59	50
6	55	9.29	17.56	4.76	8.6	50
7	56	9.99	17.45	5.67	9.3	50

Table (6.1) Experiment 3, run 1 breaking load

Test number	No. of tested samples	Mean (N)	Max (N)	Min (N)	Median	Fiber diameter (μm)
1	14	8.4	11.14	5.36	8.64	50
2	56	10.63	17.55	3.35	10.41	50
3	56	12.43	10.349	4.67	12.12	50
4	56	9.04	10.88	6.07	8.14	50
5	56	9.66	10.98	5.99	8.87	50
6	56	9.09	17.45	5.76	8.35	50
7	56	10.64	18.14	5.53	9.64	50
8	56	9.39	17.5	5.35	8.62	50

Table (6.2) Experiment 3, run 2 breaking load

For comparison reasons, a population of 235 samples, as shown in table (6.3), of virgin glass was also tested averaging about 5.3 N of breaking load, or 2.7 GPa in tensile strength for a 50 μm fiber diameter.

Test number	No. of tested samples	Mean (N)	Max (N)	Min (N)	Median	Fiber diameter (μm)
1	20	5.61	6.43	3.26	5.48	50
2	54	4.72	6.79	2.34	4.93	50
3	16	5.4	6.48	2.45	4.67	50
4	55	5.07	6.37	2	5.17	50
5	53	5.34	6.67	2.75	4.97	50
6	50	5.67	6.91	2.83	5.07	50

Table (6.3) Virgin glass breaking load

Results from Run1 and Run 2 revealed that the fibers gained significant increase in the fibers strength. The highest measured breaking load is 20 N, or 10.3 GPa in tensile strength, which indicates a 300% increase in the tensile strength, compared to the pristine glass fibers. Figure (6.6) shows the results for Run1 and Run 2. The trend of the two plots is the same with an ultimate breaking load of 20 N in both cases.

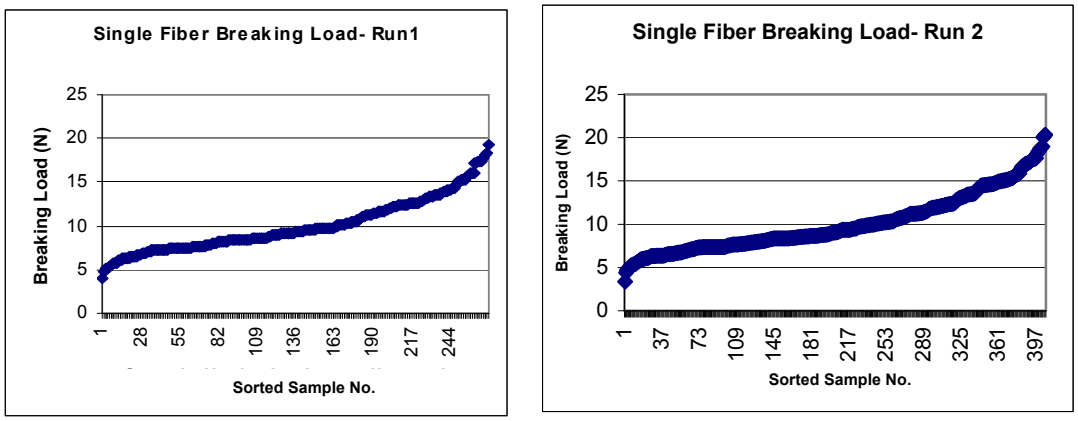

Figure (6.6) Results obtained from runs

The combined data sets for Run 1 and Run 2 are shown in figure (6.7).

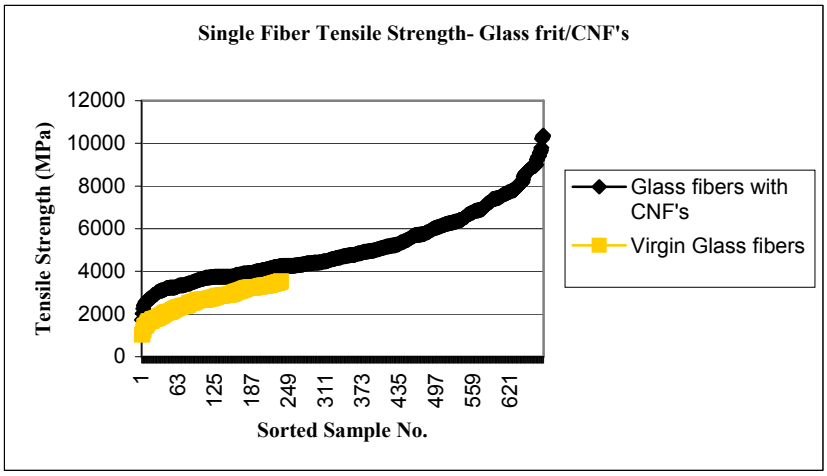

Figure (6.7) Results obtained from the third experiment

The inconsistency in the breaking load values throughout the experiment can be attributed to the following two reasons:

1. Segregation of the glass frit and the CNFs mix due to the relatively big frit size particles and the difference in densities and specific gravities between the CNFs and the glass frit. This suggests that some samples had more nano materials in their fracture surface than the others, and hence, a higher tensile strength. Also, purging Nitrogen inside the premelter caused the CNFs to scatter and separate causing more non-uniform glass frit/CNFs mix as shown in figure (6.8)

Figure (6.8) Poor mixing of glass frit with CNFs

2. When the glass frit/CNFs mix was added to the premelter, the molten glass level inside the premelter was set to 1 inch above the screen. For runs 1 and 2, the glass frit/CNFs was mixed with the molten glass before drawing the

fibers resulting in a non-uniform CNFs concentration in the glass matrix, and hence to different glass fibers strength. This is similar to doping many encapsulated CNFs coupons in the premelter, which will results in a non-uniform CNFs concentration in the mix.

The histogram plot shown in figure (6.9) shows the frequency of breaking load for virgin glass fibers and hybrid glass fibers. As it is noticed, there is clear distinction between the two types of glass fibers. The virgin glass fibers breaking load ranges between 2.5 and 6.5 N. On the other hand, the hybrid glass fibers had a wider breaking load ranging from 7.5 to 21 N. This wide trend confirms the fact that the poor mixing between CNFs and glass frit caused a variation in the CNFs concentration in the glass matrix, and hence, some samples had more CNFs in their fracture surface than others. The plot also suggests that more experiments with higher CNFs concentration are needed to more explore the region located at the right of the plot with the highest breaking load values.

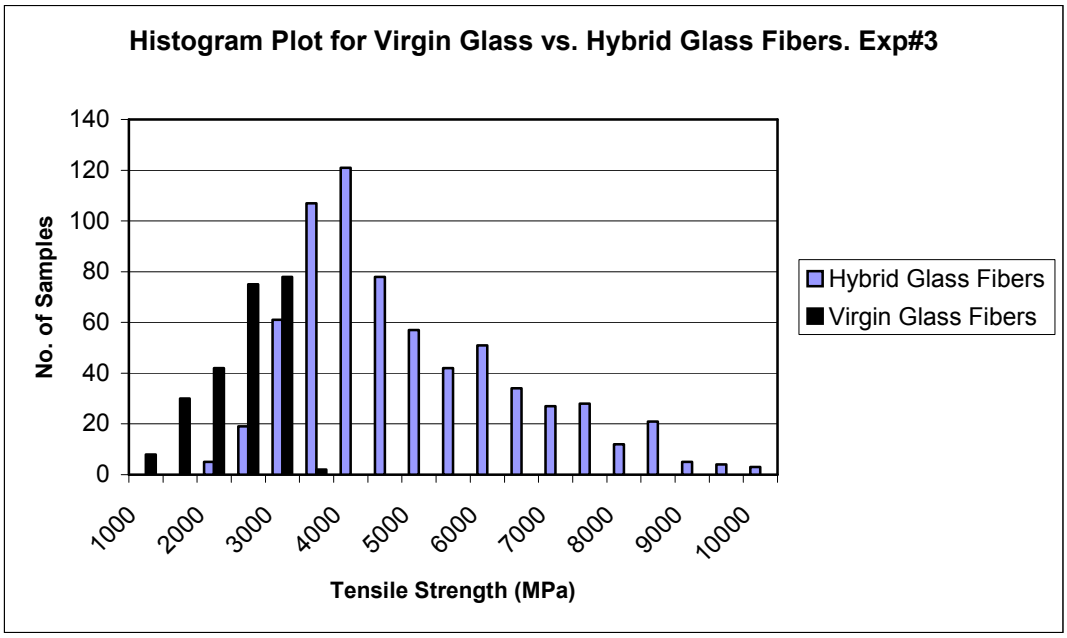

Figure (6.9) Histogram plot of tensile strength for virgin and hybrid fibers

6.5 Tensile Strength Modeling

CNFs volume fraction (V_f) was calculated using equation (4.4). The theoretical V_f values are shown in figure (6.10) with the accompanied tensile strength

values. V_f values varied from 0 to 26%, which can be verified due to the poor mixing between the glass frit and the CNFs, as a result, CNFs concentration in the mix wasn't uniform with high concentration regions. This is presented by the upper end of the plot in figure (6.9). Figure (6.11) shows the same results as %wt. CNFs.

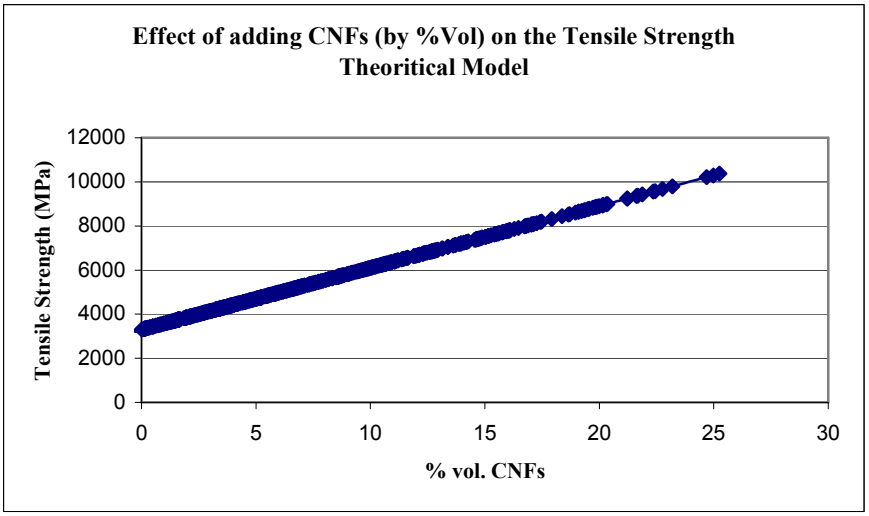

Figure (6.10) Relationship between %vol CNFs and tensile strength

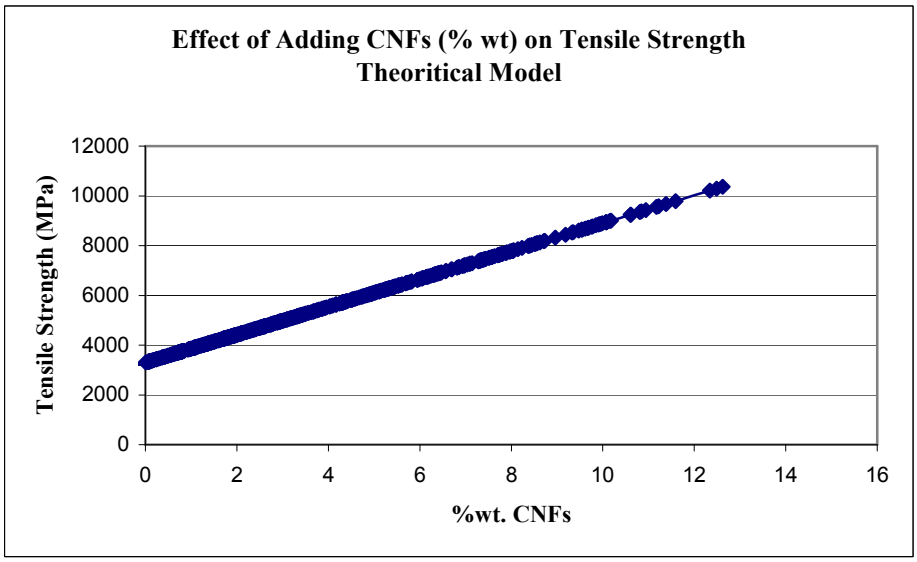

Figure (6.11) Relationship between %wt CNFs and tensile strength

Predicted σ_{com} values were calculated using equation (4.7) at different CNFs concentrations. The results are shown in figure (6.12) along with the actual measured tensile strength values. The difference between the actual vs. the theoretical values can be justified due the wide range of the tensile strength for the CNFs used in the experiment (7 to 15 GPa). In our model, it is assumed that the tensile strength for the CNFs in the composite structure is 10 GPa.

Although the predicted tensile strength looks similar to the actual one, the model described in section (4.2) is considered to be insufficient and lacks to count for many variables. The model assumes that the nano materials have a uniform concentration in the matrix and that they are aligned and continuous. These assumptions are not valid in this experiment since the CNFs are not uniformly distributed in the glass matrix besides the nano fibers are not continuous.

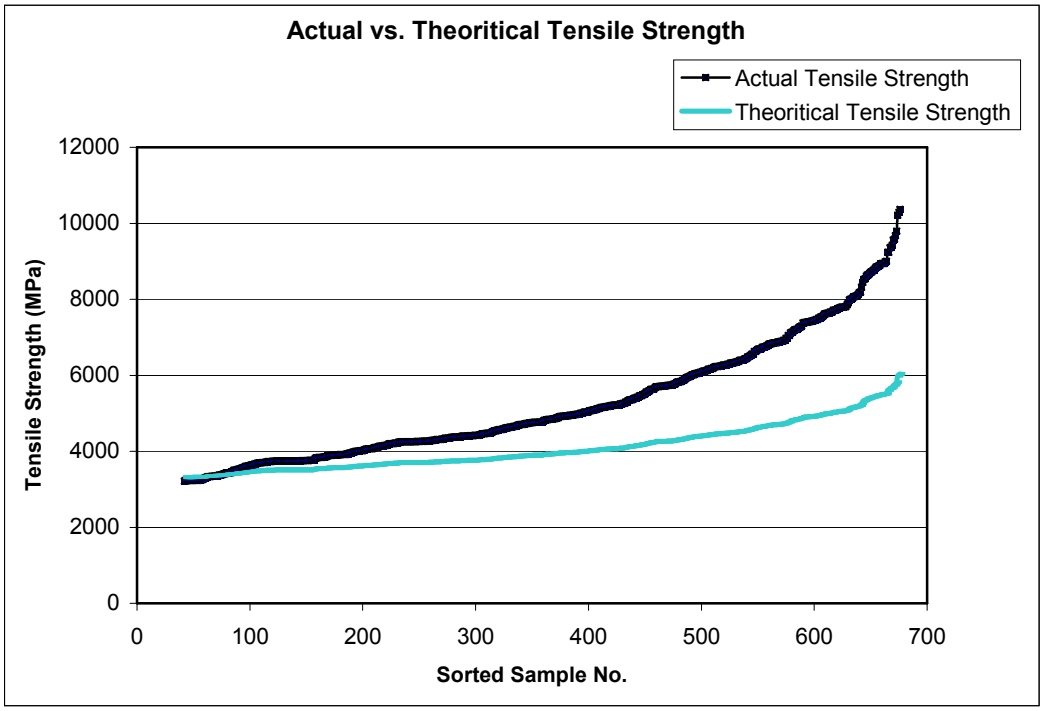

Figure (6.12) Actual vs. theoretical tensile strength

The modulus of elasticity for both the virgin glass fibers and the glass fibers mixed with CNFs was calculated using equation (4.3). The results that are shown in figure (6.13) reveal that the hybrid fibers gained, on average, 55% in their modulus of elasticity and in some cases the improvement was close to 100%.

The increase in the modulus of elasticity was due to the alignment of the carbon nanofibers during the glass forming process that resulted in improvement on the glass fibers stiffening and strengthening effectiveness.

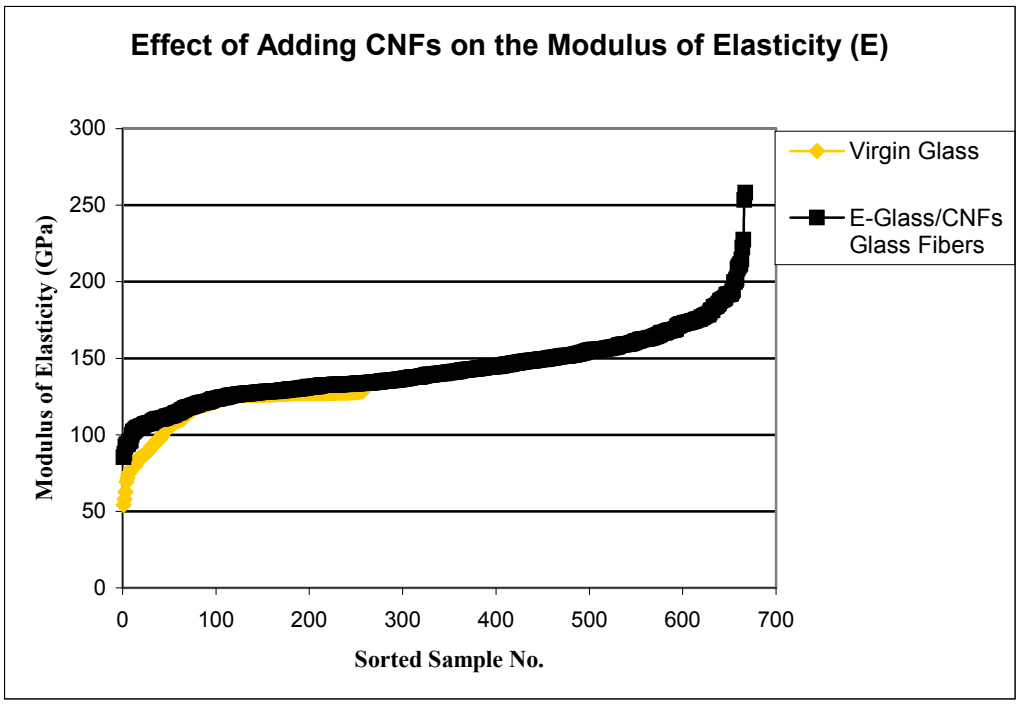

Figure (6.13) Modulus of elasticity for virgin vs. hybrid

6.6 Structural Analysis

SEM images for fibers with breaking loads between 6.5 N and 7.5 N were conducted by NASA-GRC, as shown in figure (6.14). The images didn't show, as expected, any nano materials on the fibers fracture surface. Moreover, the Energy

Dispersive Spectrometry (EDS) testing didn't show any presence of carbon in the fibers chemical composition. This confirms that those glass fibers are virgin and their tensile strength values can be considered for the comparison purposes.

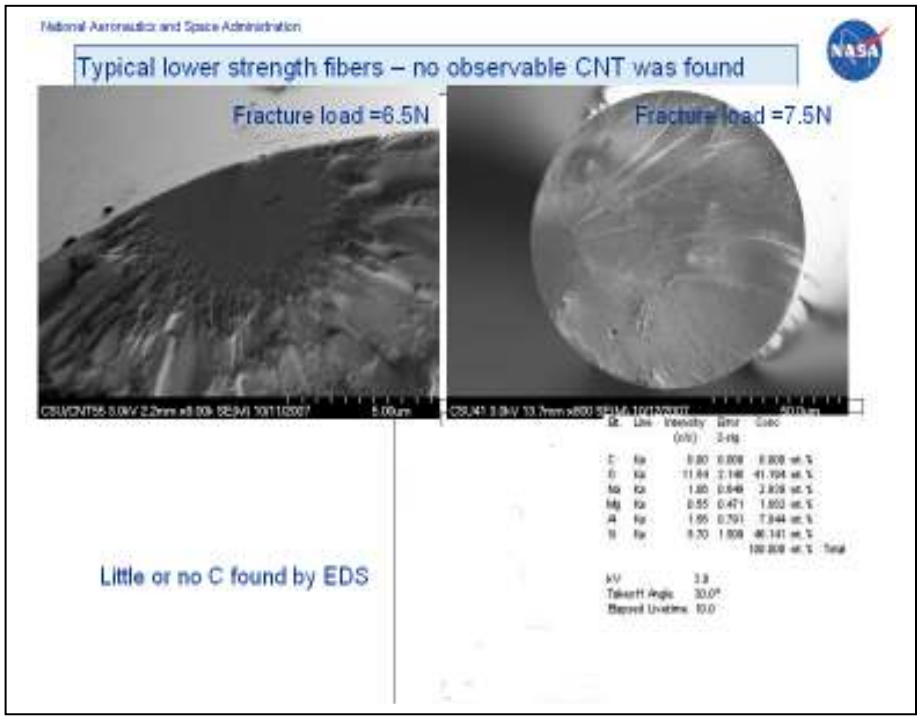

Figure (6.14) SEM Image for fibers with 6.5 N and 7.5 N

Other fibers in the range of 11 N breaking loads were also scanned and tested for their chemical composition. The SEM images in figure (6.15) show a large presence of carbon nano materials in the glass matrix. Moreover, the images show that the CNFs are well dispersed in the matrix. The toughening mechanism is also confirmed by noting the presence of broken CNFs, which suggests that the bonding forces between the glass matrix and the CNFs are strong. Other CNFs shown in the same figure were pulled out, which suggests that those CNFs were strong enough to

carry the load without breaking them, however, it also suggests that the bonding forces between the CNFs and the glass matrix were not very strong.

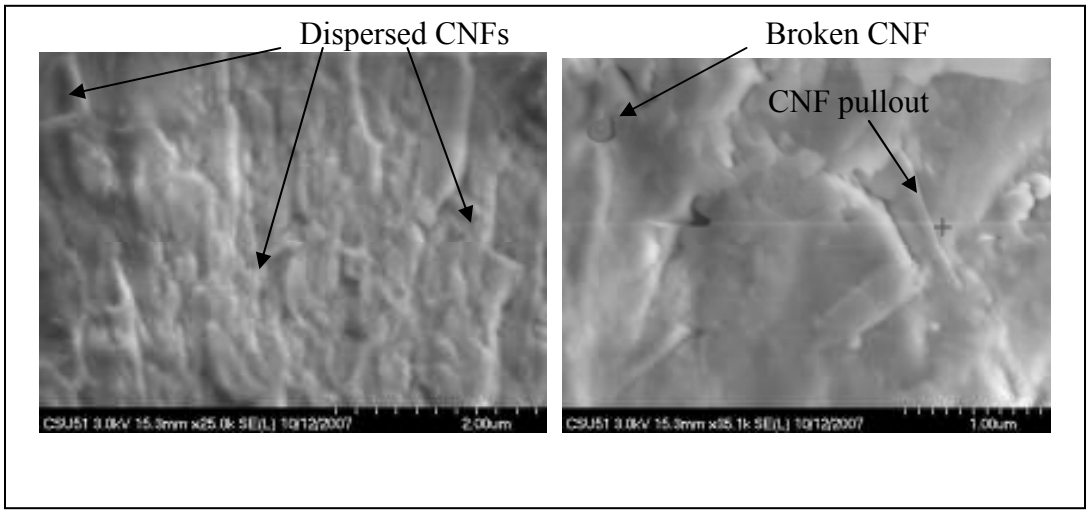

Figure (6.15) SEM images for samples with breaking load of 11 N
[Source: Janet Hurst, NASA -GRC]

Microscopic pictures for fibers from Runs 1 and 2 showed minor or no glass crystallization inside the fibers, as shown in figure (6.16). This shows that initially the CNFs had no effect on the glass forming process, however, as will be discussed later, the fibers and the experimental setup were undergoing a catastrophic chemical reaction.

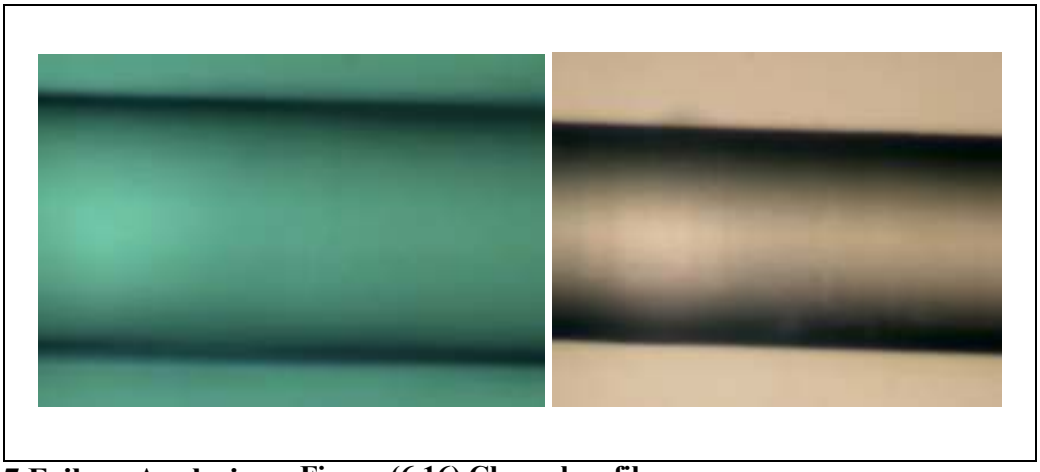

Figure (6.16) Clear glass fibers

6.7 Failure Analysis

Results from Run 3 through Run 12 showed a decrease in the tensile strength. The average breaking load for a 50 μm fiber was 3.2 N. Figures (6.17) and (6.18) show tensile strength results for runs 3 and 4. Runs 5 to 12 follow the same pattern.

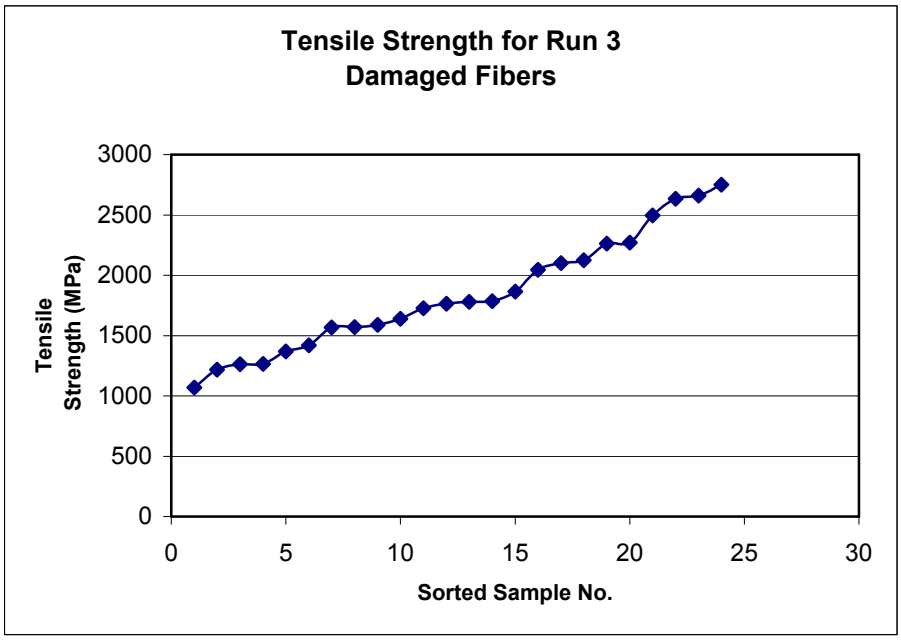

Figure (6.17) Tensile strength results for Run 3

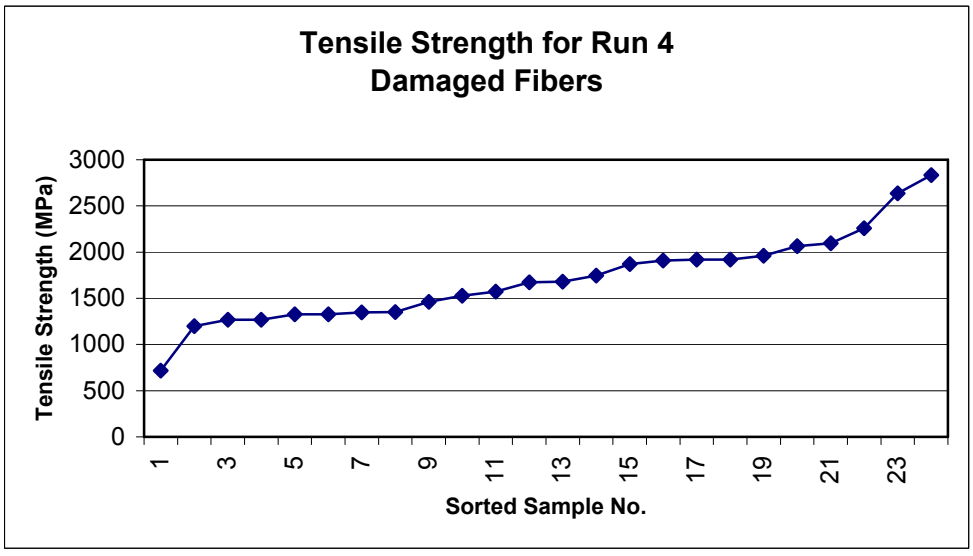

Figure (6.18) Tensile strength results for Run 4

The low mechanical properties for these fibers can be attributed to the following reasons:

1. The damage occurred to the Platinum (Pt) screen inside the premelter and the nozzles in the bushing. The damage caused the production of glass fibers with defects/voids, which lowered the fibers mechanical properties. It has not been yet determined what caused the damage, other than it's being a chemical reaction. The chemical reaction may have happened between Oxide Silica (SiO_2) from glass and Carbon (C) to form Silicon Carbide (SiC). SiC reacted with the Platinum nozzles in the bushing and the screen inside the premelter and caused the damaged shown in figure (6.19). The following explains the possible chemical reactions:

$$SiO_2 + C \rightarrow SiC + CO_x$$

$$SiC + Pt \rightarrow Pt_xSi_y \text{ or } Pt_xC_y$$

Figure (6.19) Molten premelter and nozzles

2. After the damage that happened to the premelter, purging Nitrogen created voids/channels inside the fibers. Those channels acted as high stress spots and weakened the fibers, as shown in figure (6.20).

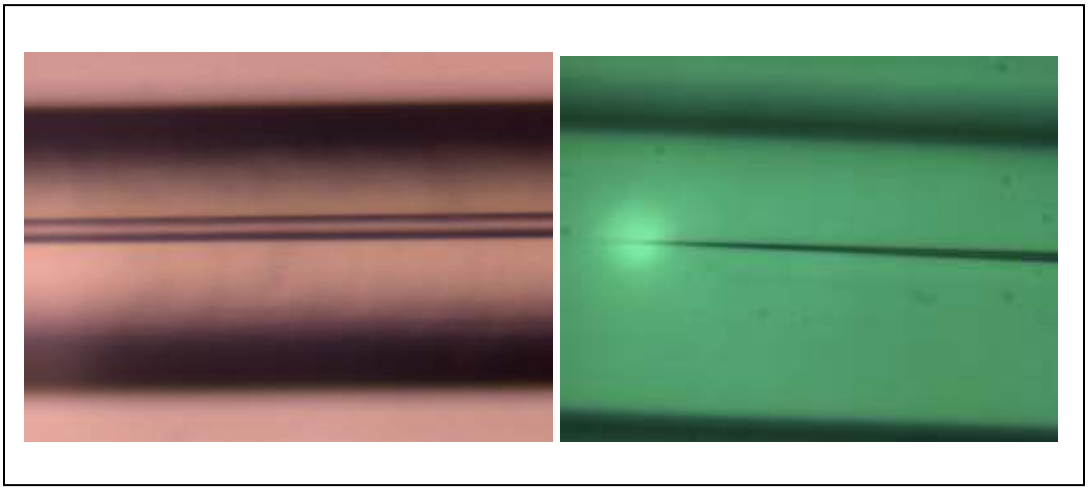

Figure (6.20) Glass fibers with air voids and channels

The molten screen caused crystallization and formed air voids inside the fibers, as shown in figure (6.12). This crystallization caused the fibers to weaken and to become brittle.

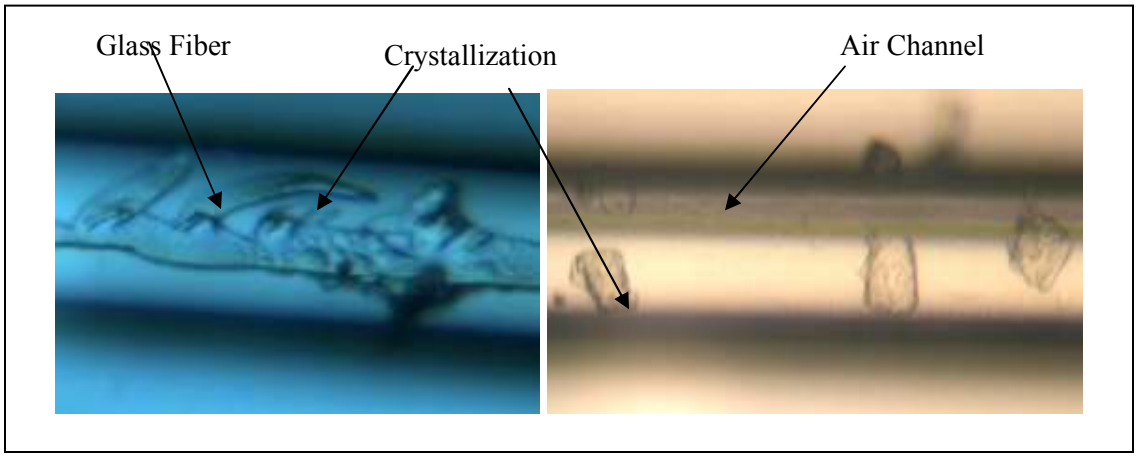

Figure (6.21) Crystallization inside the glass fibers

CHAPTER VII

CONCLUSIONS AND SCOPE FOR FUTURE WORK

7.1 Conclusions

The aim of this work was to validate utilizing the glass fibers drawing process to imbed, disperse, and align the CNFs in the glass fibers to produce hybrid glass fibers with superior mechanical, electrical and thermal properties.

Preliminary and feasibility experiments involved using hot pressed E-glass/CNFs coupons at 20% wt. CNFs. The coupons were introduced to the molten glass during the glass forming process. Structural testing, using SEM microscopy, confirmed that the CNFs survived the high temperature during the process and that they were well dispersed and aligned in the direction of glass grains. The strong

bonding interface between the CNFs and the glass matrix was confirmed by noting the pull out and the breaking of the CNFs at the fracture surfaces.

In conclusion, our observations showed that imbedded CNFs survived the high temperatures during the glass forming process in addition for being well-dispersed and aligned in the glass matrix. Tensile testing on the hybrid glass fibers showed superior fibers strength with up to 6 GPa in the case of encapsulated CNFs, and up to 10 GPa in the case of CNFs/glass frit, this can be translated into 200% and 300% improvement, respectively, on tensile strength compared to pristine E-glass which has a tensile strength of 3.2 GPa. Modulus of elasticity for the CNFs/glass frit fibers was increased by, on average, 55% and in some cases the improvement was close to 100%.

7.2 Scope for Future Work

1. *To obtain a better uniform CNFs concentration in the glass matrix, more research should be conducted that involves using glass powders instead of glass frit. Small glass particles with lower specific gravities will provide better mixing between the nano fibers and the glass powder. Similar results could also be obtained by using glass marbles with CNFs imbedded in the glass structure as feedstock to the glass fiber machine.*
2. *Higher CNFs concentrations (greater than 5% wt. CNFs) should be investigated. Our results indicated that there is a great potential of increasing the fibers strength by increasing the concentration of the imbedded CNFs.*

3. *The tensile strength of CNFs used in our experiments varied from 7-15 GPa. Other types of NTs with higher tensile properties, such as SWCNTs and MWCNTs, should be used and investigated.*
4. *Better understanding of the chemical reactions involved in the experiments, especially the reaction between SiO_2, C and Pt. that caused the catastrophic damage to the premelter/bushing during running the experiments. Also, the effect of purging Nitrogen under high temperatures during the glass fibers forming should be investigated and studied.*
5. Tensile strength modeling that involves the microstructure of the reinforced fibers should be developed. The ultimate tensile strength of a composite is affected not only by the CNFs volume fraction, but also with the microstructure of the nanocomposite. Tensile strength models that are developed so far assume that the nano reinforcement fibers imbedded in composites are continuous, unidirectionally aligned and uniformly distributed in the matrix.

REFERENCES

1. Yoshinori Ando, Xinluo Zhato, and Mukul Kumar. Growing Carbon nanotubes,
   materials today, October 2004.
2. Erik T. Thostensona, Zhifeng Renb, and Tsu-Wei Chou. Advances in the science and technology of carbon nanotubes and their composites. Composites Science and Technology 1899-1912, 2001
3. Iijima, S., Helical microtubules of graphitic carbon., Nature, 354, 56-58, 1991
4. Inpil Kang, Yun Yeo Heung, Jay H. Kim, Jong Won Lee, Ramanad Gollapudi, Suhasini Narasimhadevara, and Douglas Hurd. Introduction to carbon nanotube and nanofiber smart materials, Composites, 382-394, 2006
5. Dresselhaus MS, Dresselhaus G, Eklund PC. Science of fullerenes and carbon nanotubes. San Diego: Academic Press, 1996
6. Thess, A., Lee, R., Nikolaev, P., Dai, H., Petit, P., Robert, J., Xu, C., Lee, Y. H., Kim, S. G., Rinzler, A. G., Colbert, D. T., Scuseria, G. E., Tomanek, D., Fischer, J. E. and Smalley, R. E., Crystalline Ropes of Metallic Carbon Nanotubes., Science, 273, 483-487, 1996
7. Yacaman, M.J., Yoshida, M.M., Rendon, L. and Santiesteban, J.G., Catalytic growth of carbon microtubules with fullerene structure. Appl. Phys. Lett., 62, 202, 1993

8. Yu, M-F., Files, B.S., Arepalli, S. and Ruoff, R.S., Tensile loading of ropes of single wall carbon nanotubes and their mechanical properties., Phys. Rev. Lett. , 84, 5552-5555, 2000

9. Hone, J., Whitney, M. and Zettl, A., Thermal conductivity of single-walled carbon nanotubes., Synthetic Metals 1, 103, 2498-2499, 1999

10. Haihui Ye, Hoa Lam, Nick Titchenal, Yury Gogotsi,a) and Frank Ko. Reinforcement and rupture behavior of carbon nanotubes–polymer Nanofibers, Applied physics letters, volume 85, number 10, 2004.

11. Kuzumaki, T., Miyazawa, K., Ichinose, H. and Ito, K., Processing carbon nanotube reinforced aluminum composite., J. Mater. Res., 13, 2445-2449, 1998

12. Chen, W. X., Tu, J. P., Wang, L. Y., Gan, H. Y., Xu, Z. D. and Zhang, X. B., Tribological application of carbon nanotubes in a metal based Composite coating and composites., Carbon, 41, 215-222, 2003

13. Ruoff RS, and Lorents DC. Mechanical and thermal-properties of carbon nanotubes. Carbon. 33(7):925–30, 1995

14. Govindjee S, and Sackman JL. On the use of continuum mechanics to estimate the properties of nanotubes. Solid State Communications 110(4):227–30, 1999

15. D. M. Miller. Glass Fibers, Engineered Materials Handbook, Vol. 1 – Composites, ASM International. pp. 45-48. 1987

16. K. L. Lowenstein, The Manufacturing Technology of Continuous Glass Fibers.Elsevier, pp. 28-30, 1973

17. J. C. Watson, and N. Raghupathi, Glass Fibers, Engineered Materials Handbook. Vol. 1 – Composite, ASM International, pp. 107-111, 1987

18. Satish Kumar, Polymer/Carbon Nanotube Composites: Challenges and Opportunities. School of Polymer, Georgia Institute of Technology.

19. Thaliyil Sreekumar, Tao Liu, Byung G, and Robert Hauge, Polyacrylonitrile single walled carbon nanotube composite fibers. Advanced materials, 16, no 1, 2004

20. Biercuk, M. J., Llaguno, M. C., Radosavljevic, M., Hyun, J. K., Johnson, A. T. and Fischer, J. E., Carbon nanotube composites for thermal management., Appl. Phys. Lett.,, 80, 2767-2769, 2002

21. Choi, E. S., Brooks, J. S., Eaton, D. L., Al-Haik, M. S., Hussaini, M. Y., Garmestani, H., Li, D. and Dahmen, K., Enhancement of thermal and electrical properties of carbon nanotube polymer composites by magnetic field processing., J. Appl. Phys., 94, 6034-6039, 2003

22. Gojny, F. H., Wichmann, M. H. G., Koepke, U., Fieldler, B. and Schulte, K., Carbon nanotubes-reinforced epoxy-composites: enhanced stiffness and fracture toughness at low nanotubes content., Compos. Sci. Technol., 64, 2363-2371, 2004

23. Qian, D., Dickey, E. C., Andrews, R. and Rantell, T., Load transfer and deformation mechanisms in carbon nanotube-polystyrene composites., Appl. Phys. Lett., 76, 2868-2870, 2000

24. A.R. Boccaccini, D.R. Acevedo, and G. Brusatin, P. Colombo, Borosilicate glass matrix composites containing multi-wall carbon nanotubes. Journal of Europe Society, 1515-1523, 2005

25. Jinwei Ning, Junji Zhang , Yubai Pan, and Jingkun Guo, Fabrication and mechanical properties of SiO2 matrix composites reinforced by carbon nanotube. Materials Science and Engineering A357, 392-396, 2003

26. Yuji Katsuda, Peter Gerstel , Janakiraman Narayanan , Joachim Bill , and Fritz Aldinger. Reinforcement of precursor-derived Si–C–N ceramics with carbon nanotubes. Journal of the European ceramic society 26, 3399-3405, 2006.

27. Feng Ye, Limeng Liu, Yujin Wang, Yu Zhou, Bo Peng and Qingchang Meng. Preparation and mechanical properties of carbon nanotube reinforced barium luminosilicate glass–ceramic composites, Scripta Materialia, 911-914, 2006

28. Mitch Jacoby, Borion Nitride Nanotubes formed. News of the week science, Vol. 19, number, 12, pp. 10, 2001

29. L.R. Vishnykov, .V. Maznaya, L.N. Pereselentseva, and B.N. Sinaiskii. Structure and high-temperature strength of composite materials based on boron nitride. Powder metallurgy and metal ceramics, Vol 45, Nos. 5-6, 2006

30. G. I. Savvakin, T. V. Dubovik, and G.S. Oleinik. Structural study of ceramics based on graphite-like boron nitride subjected to detonation treatment. Poroshk Metal, Nos. 5-6, 75-80, 1995

31. Masa Ishigami, Shaul Aloni, and A. Zettl. Properties of boron nitride nanotubes, University of California at Berkley, 2004

32. Narottam P. Bansal, Janet B. Hurst, and Sung R. Choi. Boron Nitride Nanotubes-Reinforced Glass Composites. NASA/TM- 213874, 2005

33. G. M. Song, Y. Zhoun, and Y. Sun. Modeling of fiber toughening in fiber-reinforced ceramic composites. Ceramics international, 257-260, 1999

34. V. C. Li, and C. K. Leung, ASCE journal of engineering mechanics, 118 2246, 1992

35. M. Maalej, Tensile properties of short fiber composites with fiber strength distribution. Journal of materials science 36, 2203-2212, 2001

36. Kadolph, Sara J., and Anna L. Langford. Textiles Ninth Edition. New Jersey: Prentice Hall, 1998.

37. Top U.S. Monthly Imports. Nonwovens Markets, Vol. 21 Issue 7, p4-5, 2006

38. J.J. Sha, J.S.Park and T. Hinoki. Strength and fracture properties of advanced SiC based fibers, Mechanics of composite materials, Vol 42, No. 6, 2006

39. A.Suciu, G. Civelekoglu, and J.J Meister, Model for the alignment of acting filaments in endothelial cells subjected to fluid shear stress, Bulletin of mathematical biology, Vol 59, pp. 1029-1046, 1997

40. Sandler, J.K.W., Shaffer, M.S.P., Prasse, T., Bauhofer, W., Schulte, K. and Windle, A.H., Development of a dispersion process for carbon nanotubes in an epoxy matrix and the resulting electrical properties., Polymer, 40,

5967-5971, 1999

41. Lau, K.T. and Hui, D, Effectiveness of using carbon nanotubes as nano reinforecement for advanced composite structure, Carbon 1597-1617, 2002

42. P. Poulin, and P. Launois, Carbon (40), 1741, 2002

43. Youngmin Lee, Sangkwan Lee, Y. Jang and Sangshik Kim, Unidirectional alignment of carbon nano-sized fiber using drawing process, Journal of Materials Science (40), 6037-6039, 2005

44. Carole Cooper, D. Ravich, Joerg Mayer, and Daniel Wagner, Distribution and alignment of carbon nanotubes and nanofibrils in a polymer maytrix, Composites science and technology (62), 1105-1112, 2002

45. Massey, B. S, Mechanics of Fluids, fifth edition, 1983

46. L. C. Saw yer, M. Jamie son, D. Brikowski, M. I. Haider, and R. T. Chen, J. Amer. Ce ramic Soc., 70, 798-810 1987.

47. M. D. Thouless, O. Sbaizero, L. S. Sigl, and A. G. Ev ans, J. Amer. Ce ramic Soc., 72, 525-532 (1989)

48. F.T. Wallenberger, Structural Silicate and Silica Glass Fibers, in Advanced Inorganic Fibers Processes, Structures, Properties, Applications, F.T. Wallenberger, Ed., Kluwer Academic Publishers, p 129–168, 1999

49. F.T. Wallenberger, Melt Viscosity and Modulus of Bulk Glasses and Fibers: Challenges for the Next Decade, in Present State and Future Prospects of Glass Science and Technology, Proc. of the Norbert Kreidl Symposium (Triesenberg, Liechtenstein), p 63–78,1994

50. Douglas C. Montgomery, Design and Analysis of Experiments, John Wiley & Sons, Fifth edition, 2001

51. Taysir Nayfeh and Janet Hurst (NASA Glenn Research Center, Cleveland, OH), Patent Pending, 2007

52. Alain Burr and Hild, Ultimate tensile strength during fatigue of fiber-reinforced ceramic-matrix composites, Mechanics Research Communications, Elsevier, 0093-6413/95,1995